

Stress and strain field at volcanoes under consideration of material heterogeneities

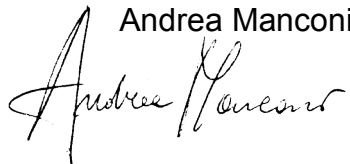
Dipl.-Ing. Andrea Manconi

Thesis submitted for the degree of Doctor rerum naturalium

**Institut für Geowissenschaften, Universität Potsdam,
Karl-Liebknecht-Strasse 24, Haus 27, 14476 Potsdam, Germany
March, 2009**

I herewith declare that I have produced this paper without the prohibited assistance of third parties and without making use of aids other than those specified; notions taken over directly or indirectly from other sources have been identified as such. This paper has not previously been presented in identical or similar form to any other German or foreign examination board. This work has been financially supported by the German Research Foundation (DFG) through the grant WA1642-1/4 and the GFZ German Centre for Geosciences.

Potsdam, 04.03.2009

Andrea Manconi


...ma l'ha detto "Dottore" ? Eh si, mi sa che stavolta lo ha detto davvero...

Acknowledgements

During the PhD period I had the possibility to interact and collaborate with a number of people, which in different ways contributed to my growth as a man and as a scientist. First of all thanks to Thomas Walter, who gave me the possibility to make such an exiting experience in an active and multidisciplinary environment as the GFZ Potsdam. Thanks a lot, because what I did here it has been more than what I expected for my PhD project: a combination of numerical modeling, fieldwork, and experiences with students, international collaborations and participation at international conferences. I will never forget its door always open for long discussions and the “systematic” that will always remain impressed on my way-to-work. Thanks to the all section 2.1 of the GFZ Potsdam, always ready to share their experience and to give invaluable suggestions. Special thanks go to Francisco Lorenzo, for me a mentor in giving the right initial tips to approach the PhD period, but especially a friend outside the working environment. Many thanks to Stefano Parolai and Dino Bindi, for the constructive and critical comments that broadened my view of geophysical problems, my capacity of analysis and of understanding. For the same reason, thanks to Angelo Strollo, Matteo Picozzi and Domenico Di Giacomo, but also for being always ready to help me in many situations of my life at work and outside. Thanks to the several people who had internships period within our group. Especially to Marc-Antoine Longpré, for the intense collaboration which will surely remain beyond a simple co-authorship in a paper. Thanks to Prof. Schmincke, who has shown me “the beauty of volcanoes” at Gran Canaria during the Volcanology field school in the summer 2006.

Very special thanks go to Joël Ruch, with whom I shared large part of my time, ideas and thoughts, scientific and not. The periods in the field in Chile and in Iceland will be indelible in my mind. It is somehow particular to have so much empathy (professional and human) with somebody coming from completely different backgrounds and experiences. Well, may be is because Sardinia and Switzerland are both Islands, aren't them?

My final thoughts are for my family, which always supported in every situation my efforts. But my infinite gratitude goes to Paola. She enjoyed with me my achievements. She carried my stressful periods and my frustrations with inestimable patience and sustained me with love. She knew from the beginning how was important for me, and I am sure she is glad that now is over! However, with some egoism, all the work I have done in these years of studies since the beginning of the university until the aspiration to the doctoral degree is finally dedicated to myself. Sometimes, for a number of reasons, it would have been really easier to give up...nevertheless you got it.

Table of contents:

ABSTRACT	8
GENERAL INTRODUCTION	9
CHAPTER 1	11
1.1. THE FINITE ELEMENT METHOD	11
1.2. WHY FEM IN VOLCANO-TECTONICS?	12
CHAPTER 2	14
THE EFFECTS OF FLANK COLLAPSES ON VOLCANO PLUMBING SYSTEMS	
<i>ABSTRACT</i>	14
2.1. <i>INTRODUCTION</i>	15
2.2. <i>BACKGROUND</i>	16
2.3. <i>FINITE ELEMENT MODELS</i>	18
2.4. <i>SUMMARY AND DISCUSSION</i>	21
CHAPTER 3	26
EFFECTS OF MECHANICAL LAYERING ON VOLCANO DEFORMATION	
<i>ABSTRACT</i>	26
3.1. <i>INTRODUCTION</i>	27
3.2. <i>MODELING</i>	29
3.3. <i>APPLICATION TO DARWIN VOLCANO</i>	35
3.4. <i>DISCUSSION</i>	38
3.5. <i>CONCLUSIONS</i>	41
CHAPTER 4	43
THE SOURCE OF GROUND DEFORMATION AT CAMPI FLEGREI CALDERA DURING THE LAST 16-YEARS: INSIGHTS FROM FINITE ELEMENT MODELING AND SBAS-DInSAR TIME SERIES ANALYSIS	
<i>ABSTRACT</i>	43
4.1. <i>INTRODUCTION</i>	44
4.2. <i>FINITE ELEMENT MODELS OF CF CALDERA</i>	47
4.3. <i>APPLICATION TO GROUND DEFORMATION MEASURED AT CF CALDERA</i>	51
4.4. <i>SUMMARY AND DISCUSSION</i>	56
4.5. <i>CONCLUSIONS</i>	62
4.6. <i>APPENDIX</i>	63
FINAL REMARKS AND FUTURE RESEARCH DEVELOPMENTS	67
GSA DATA REPOSITORY: SUPPLEMENTARY INFORMATION FOR CHAPTER 2.....	69
REFERENCES	81
CURRICULUM VITAE	91

Abstract

Volcanic activity is the surface expression of a number of complex physical phenomena occurring in the Earth's interior. In volcanology, as well as in other geophysical branches, the linkage between surface observations and the deep-seated processes is explained through models. Most of the modeling attempts in volcanology are still made assuming the Earth's crust as a homogeneous and elastic half-space. This simplification is often necessary in areas where the knowledge of subsurface properties is poor. However, at volcanoes mechanical heterogeneities are clearly recognized from geological and geophysical studies, i.e. the assumption of homogeneity is likely misleading the derived interpretations.

In this work we analyze into details such problematic, focusing our research mainly on the study of two volcano-tectonic processes: the collapse of portions of the volcanic edifices and the surface deformation caused by volcanic unrest. Using the Finite Element Method (FEM), a numerical technique mostly used in advanced engineering applications, we introduced within the models realistic material mechanical parameters, and performed systematic studies in order to understand their effects on stress and strain field. Our results suggest that material heterogeneities have to be taken into account for a correct interpretation of volcano-tectonic-processes. The herein presented specific and general implications provide a basis for more complex modeling attempts, which are likely to be developed in many future applications.

General introduction

The main goal of this study is to understand how the interpretations of some volcano-tectonic processes, usually performed using homogeneous models, may change under the consideration of more realistic mechanical properties. After a brief introduction about the finite element method (chapter 1), a number of different problems will be analyzed:

- The effects of volcanic flank collapses on volcano plumbing system processes (chapter 2).
- The effects of mechanical layering on the interpretation of surface deformation in volcanic areas (chapter 3).
- The influence of a realistic 3-D distribution of mechanical heterogeneities on surface deformation at Campi Flegrei caldera, Italy, and the implications for the understanding of its ground deformation revealed in the last sixteen years (chapter 4).

The methodologies, results and interpretations presented in this study are based on a compilation of three papers. At the time of writing, one paper is under review in *Geology* (Manconi et al., chapter 2), one has been already published in the *Geophysical Journal International* (Manconi et al., 2007, chapter 3), and the third has been recently submitted to the *Journal of Geophysical Research* (Manconi et al., chapter 4). In all the works, I have been the principal investigator. Details about the singular contributions of all co-authors to the above-mentioned papers will be explained at the beginning of the related chapters.

CHAPTER 1

1.1. THE FINITE ELEMENT METHOD

The Finite Element Method (FEM) is an advanced numerical technique firstly applied in the 1950s in structure mechanics, and progressively becoming an extremely flexible tool for solving numerous engineering problems. The developments of the FEM have been clearly related to the rapid advances of the computer technology and consequent increase of the computational capabilities. In general, the FEM might be introduced rigorously, with the theory developed to obtain approximated solutions of Partial Differential Equations (PDE). However, herein are presented only the basic principles of the technique, which are straightforward and rather easy to understand.

The first phase implies the definition of the problem, usually associated with the description of the geometrical characteristics of the domain of interest (DOI). The latter is thus discretized in a number of sub-domains, or “elements”, which are interconnected through common points, or “nodes”. After the discretisation of the DOI, the governing mathematical relationships defining the physics of the problem have to be assembled to give a system of equations. A set of boundary conditions provides constraints to describe the behavior of the body as a whole. After solving the unknown nodal values, the results are finally averaged and might be post-processed, in order to get insights from the performed analysis. Since by means of the FEM we achieve an approximated solution of the real problem, the results of the analysis have

to be either compared with the analytical solution (if existing) or benchmarked through a convergence test. The former requires an increase of the number of elements, thus of the degrees of freedom of the system, until the attained numerical solution appears stable.

Nowadays a number of commercial packages include sophisticated graphical interfaces that allow an easy-and-fast implementation of the FEM even for very complex problems, which would be probably rather difficult to approach without. Moreover, post-processing tools may produce visually exciting output with a minimum input from the user. However, it has always to be reminded that the validity and the accuracy of the results of a finite element analysis depend on a rigorous representation of the problem and on a correct understanding of the physics of the studied processes. Further details about the technique, the procedures and several applications can be found in Fagan, 1992.

1.2. WHY FEM IN VOLCANO-TECTONICS?

Volcanoes are geological features characterized by complex geometrical shapes, by the presence material heterogeneities, and by the coexistence of number of physical processes that contribute to their activity and evolution. In general, the use of simplified models to describe complex coalescent processes may bias the final interpretations, hence the correct understanding of the phenomena. In this context, the FEM is particularly suitable for the analysis of a “Multiphysics environment” like volcanoes. This might include steady state (static analyses, e.g. stress-strain under elastic regime) as well as transient problems (time-dependent analyses, e.g. stress-strain under plastic and viscoelastic regime). The geodetic measurements of the surface deformation due to volcanic unrest, the seismic events due to fracturing processes and fault reactivation, the measures of the gas emissions of the magmatic and/or hydrothermal system, and the petrographic analysis of the erupted products, may provide constraints for the finite element modeling attempts. As previously mentioned, however, the reliability of the results obtained using the FEM depends on the capability to well represent in the

“computer-space” the real problem of interest. In volcano-tectonics, and generally in geosciences, this usually comports a number of assumptions and simplifications that have to be taken into account and thus “a priori” carefully evaluated. All the modeling attempts included in this work are yet based on the assumption of elastic regime. The model limitations and the validity of the approximations will be discussed in turn in every chapter and more in general in the concluding remarks. Nevertheless, the conclusions derived with the application of the here presented finite element models are relevant in the present context, and provide a basis for the future correct analysis and understanding of volcano-tectonic processes.

CHAPTER 2

The effects of flank collapses on volcano plumbing systems[†]

Andrea Manconi¹, Marc-Antoine Longpré², Thomas R. Walter¹, Valentin R. Troll^{2,3} and Thor H. Hansteen⁴

(1) GFZ German Research Centre for Geoscience, Potsdam, Germany; (2) Trinity College Dublin, Dublin, Ireland; (3) Uppsala University, Uppsala, Sweden; (4) IFM-GEOMAR, Kiel, Germany

ABSTRACT

The growth of large volcanoes is commonly interrupted by episodes of flank collapse that may be accompanied by catastrophic debris avalanches, explosive eruptions and tsunamis. El Hierro, the youngest island of the Canary Archipelago, has been repeatedly affected by such mass-wasting events in the last 1 Ma. Our field observations and petrological data suggest that the largest and most recent of these flank collapses – the El Golfo landslide – likely influenced the magma plumbing system of the island, leading to the eruption of higher proportions of denser and less evolved magmas. The results of our numerical simulations indicate that the El Golfo landslide generated pressure changes exceeding 1 MPa down to upper mantle depths,

[†] **Author contributions:** T.R.W., V.R.T and T.H.H. initiated the project and facilitated the research. A.M. carried out the finite element modelling, M.-A. L. conducted the fieldwork and petrological analyses. All the authors contributed to the hypotheses and the interpretations presented. Writing and illustrating was done by A.M. and M.-A. L., with the cooperation of all authors. This manuscript is under review in *Geology*.

with local amplification in the surroundings and within the modeled magma plumbing system. Stress perturbations of that order might drastically alter feeding system processes, such as degassing, transport, differentiation and mixing of magma batches.

2.1. INTRODUCTION

Catastrophic, large-scale flank collapses punctuate the evolution of many volcanic edifices. Modern volcanology took a quantum leap in the aftermath of May 18th, 1980, as Mount St. Helens (Washington State, USA) was the site of the largest flank collapse and one of the most spectacular volcanic eruptions in recorded history. Since then, evidence of such flank collapse, in the form of amphitheatre-like re-entrants carved into volcanic edifices or remnants of related slump and debris avalanche deposits, has been identified at numerous stratovolcanoes (McGuire, 1996). Oceanic shield volcanoes too are subjected to flank collapse during their lifetime. While lateral collapses on continental stratovolcanoes generally have volumes of 10^3 - 10^5 m³ with worldwide repeat intervals of 10^2 - 10^3 years, giant slumps on oceanic islands involve volumes as large as 10^9 - 10^{12} m³ and recur every 10^4 - 10^6 years (McGuire, 1996). Due to their enormous destructive potential, volcano flank collapses and associated hazards require a sustained level of research on their causes and effects (Siebert, 1984; McGuire, 1996).

The collapse of a volcano flank has probably permanent effects on the edifice's morphology as well as on the local volcano-tectonic regime (Lipman et al., 1991). Recent studies indicate that flank collapse events at both stratovolcanoes and oceanic shield volcanoes may be followed by rapid constructional phases and changes in erupted lava compositions (Hildenbrand et al., 2004). These apparent variations in the volcanic and magmatic regimes are thought to be due to the static decompression at depth after surface unloading and its potential influence on magma chamber processes (Pinel and Jaupart, 2005), and perhaps even on mantle melt production (Presley et al., 1997). This is by analogy similar to the effect of ice unloading during deglaciation periods in Iceland that has been shown to

drastically affect local volcanism (Sigvaldason et al., 1992; Jull and McKenzie, 1996). However, no quantitative models have yet tested the postulated relationships between volcano flank collapse and subsequent volcanism.

Our field observations and the analysis of volcanic products summarized in this paper suggest that a large and recent flank collapse, the El Golfo landslide, likely affected the magmatic regime of El Hierro Island, in the Canary Archipelago. We present finite element models that simulate the unloading of realistic fractions of a volcanic edifice, using El Hierro as an exemplary case. The modeling results show that the decompression generated by the collapse of fractions of a volcanic edifice are able to induce pressure gradients and instability in a magma storage zone and its surroundings, probably accounting for drastic effects on magma plumbing and eruptive dynamics.

2.2. BACKGROUND

El Hierro is the youngest, smallest and westernmost of the Canary Islands (Fig. 2.1), and currently is in its “shield-stage period” (Carracedo et al., 2001). The island is formed by a group of coalescent volcanoes, which all show evidence of mass-wasting events. The oldest, now concealed Tiñor collapse (882-545 ka) preceded the El Julán landslide (ca. 130 km³, ca. 200 ka) that affected the southwest side of the island. In addition, two of the most recent large-scale flank collapses on Atlantic volcanoes occurred on El Hierro. The Las Playas debris avalanche (25-50 km³, between 176-145 ka) formed a prominent coastal embayment on the southeast flank of the island. Most recently, however, the El Golfo landslide (bracketed between 134-21 ka, 150-180 km³, Masson et al., 2002) removed an enormous portion of El Hierro’s northwest flank, producing a vast and well-preserved scar – the El Golfo embayment.

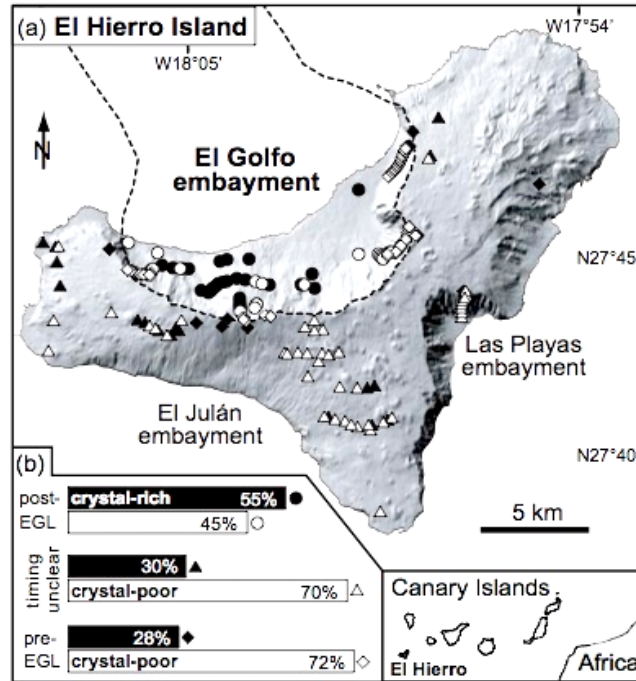


Figure 2.1: Shaded relief map of El Hierro Island. (a) Dashed lines show the extent of the El Golfo landslide (EGL) scar and deposits. Symbols represent sampling and/or investigated outcrop localities. (b) Histogram showing that ankaramitic, “crystal-rich” volcanics (black bars) have out-proportioned eruptions of all other lava types (white bars) in the recent, post-EGL volcanic phase of El Hierro.

The magma plumbing system feeding volcanism at El Hierro was recently investigated, using clinopyroxene-melt thermobarometry (Stroncik et al., 2008). Phenocrysts retrieved from submarine lava flows yield crystallization depths in the range of 19 to 26 km below sea level, suggesting that magmas are stored in a multi-level plexus of dyke- and sill-like fractures in the uppermost mantle. Moreover, the crystals’ complex zoning patterns indicate that mixing of moderately evolved and mafic magmas is an important process beneath El Hierro (Stroncik et al., 2008).

2.2.1. Field and petrological evidence

We conducted detailed field campaigns on El Hierro to determine whether the El Golfo landslide may have had observable effects on subsequent volcanism. Mapping of lava type distribution, logging of well-exposed stratigraphic sections and sampling were carried out at strategic localities on the island, particularly in the vicinity of the El Golfo embayment. Our field and

petrological analysis indicates that, from about 261 to 176 ka, the volcano emitted differentiated products, including lavas and block and ash flows of trachytic composition (up to 60 wt% SiO₂ and 0.9 wt% MgO, cf. Carracedo et al., 2001). Post-landslide eruptions, however, involved significantly more mafic magmas (mean of 44 wt% SiO₂ and 8.5 wt% MgO), that were often charged with abundant and large olivine and clinopyroxene crystals. Eruptions of these crystal-rich lavas (>20 vol. % clinopyroxene + olivine, hereafter referred to as ankaramites) appear to have outnumbered eruptions of other lava types in the recent post-landslide eruptive phase (Fig.1b). Magma density calculations indicate that ankaramites are substantially denser than other El Hierro magma types, with $\rho=2,950\pm50$ kg/m³ compared with 2,810±80 kg/m³ for moderately-phyric basalts, 2,660±60 kg/m³ for aphyric basalts and 2,390±40 kg/m³ for trachytes. For more details about the field and the petrological data, see GSA Data Repository, Section 1.

These results suggest that the recent flank collapses – most particularly the El Golfo landslide – have considerably disturbed the island’s magmatic regime, apparently causing higher proportions of considerably denser and less evolved magmas to erupt.

2.3. FINITE ELEMENT MODELS

To verify whether the perturbations of El Hierro’s volcanic regime might indeed be related to the effects of a large-scale mass-wasting, we constructed finite element models using the El Golfo landslide as a collapse type-example (Fig. 2.2a). We modeled El Hierro Island as a conical edifice loading the oceanic lithosphere, which is represented as an elastic half-space. We then removed 3% of the island’s initial weight, corresponding to the geological estimations of the El Golfo landslide (Masson et al., 2002). The simulations were first performed assuming homogeneous material throughout. Secondly, we introduced a mechanically softer region, oblate in shape (semi-axes ratio 2/5 km) and centered at a depth of 20 km below the sea floor, aiming to model the upper mantle magmatic system of El Hierro (Stroncik et al., 2008). The elastic properties of this “zone” were assumed to be dependent on the

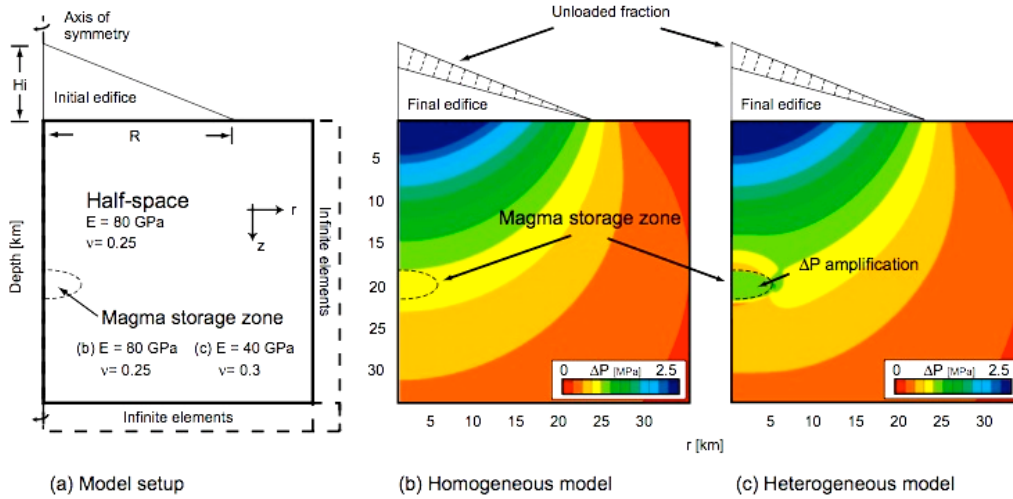


Figure 2.2: Finite element models (FEM) of the El Golfo landslide unloading the El Hierro edifice. (a) FEM Setup. The initial edifice rises above the seafloor (height (H_i)= 6 km, radius (R)=30 km). Far-field boundary conditions are simulated by imposing a set of infinite elements at the bottom and on the right side of the model. The resolution of the elements in the near-field is 100 m. Elastic properties of the half-space are defined by Young's modulus (E) and Poisson's ratio (ν). (b & c) Pressure changes after unloading within homogeneous and heterogeneous models, respectively. In (c), local stress gradients are observed inside and in the surroundings of a mechanically softer zone (dashed line) that simulates the magma storage region.

percentage of melt present within it (Ryan, 1980). Variations of mean stress at depth are defined as:

$$\Delta P = -\frac{1}{3}\sigma_{kk} \quad (2.1)$$

where σ_{kk} is the trace of the stress tensor and ΔP is hereafter referred to as decompression.

2.3.1. Modeling Results

The surface unloading caused by the El Golfo landslide induces decompression of the lithosphere at amplitudes that decay exponentially with depth (Fig. 2.2b). The pressure drop of about 4 MPa directly beneath the El Hierro edifice decreases to about 0.5-0.6 MPa at the main magma storage levels (18-22 km depth). Heterogeneous models (Fig. 2.2c) show that large pressure gradients develop in the surroundings of, as well as within, the softer magma reservoir. Decompression in this zone differs by up to 50% from that

obtained within a homogeneous half-space. Higher melt percentages cause larger gradients of decompression in the reservoir's surroundings due to a decrease of the effective elastic stiffness and to an increase of the effective incompressibility (Ryan, 1980).

Within the modeled magma plumbing system, volumetric expansion occurs and reaches up to 30 μ strain. Larger values in the upper levels of the magma storage zone compared to its lower parts lead to pressure gradients of about 0.1 MPa (Fig. 2.3a-b). The pattern and the amplitude of this differential pressure are not significantly affected when different depths, mechanical contrasts and/or various shapes of the magma reservoir are considered. Additional tests have been systematically carried out to assess the effect of different input parameters, and are detailed in the GSA Data Repository, Sections 2-4.

Our models thus suggest that the El Golfo landslide induced pressure changes and gradients at depth within El Hierro's magma reservoirs, providing likely candidates for sudden disturbances of magma plumbing dynamics.

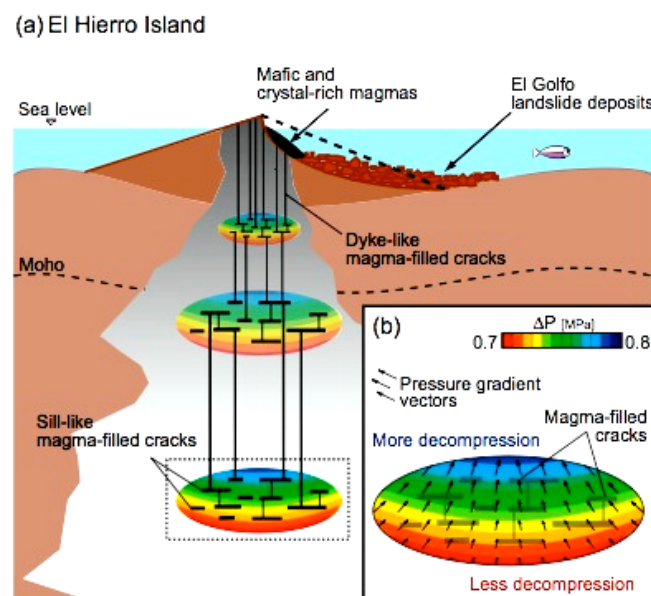


Figure 2.3: Sketch of the El Golfo landslide and its potential effects on El Hierro's magma plumbing system. (a) Broad magma storage regions beneath El Hierro are represented as oblate-shaped reservoirs. Black solid lines represent sill- and dyke-like magma-filled fractures (cf. Stroncik et al., 2008). (b) Details of a magma storage zone located at about 20 km below the sea floor (dashed rectangle in (a)). Decompression induces magma degassing, and pressure gradients that favor the remobilization, ascent and mixing of different magma batches (black arrows).

2.4. SUMMARY AND DISCUSSION

Recent studies have shown that static and/or dynamic volumetric expansion associated with earthquakes can trigger volcanic unrest. Volatile exolution, bubble nucleation and mingling and mixing of different magma batches are encouraged, thus increasing the probability of eruption (Manga and Brodsky, 2006). According to our models, the El Golfo landslide would have caused permanent volumetric expansion up to 5 times larger than that inferred for Córdon Caulle, a volcano in the Central Andes, where an eruption was triggered after the 1960 Mw 9.5 mega-thrust earthquake in Chile (Walter and Amelung, 2007). Moreover, we have shown that material mechanical contrasts are likely to play an important role in the amplitudes of landslide-induced decompression. The net mechanical contrast between the magma storage region and the surrounding rock is a key-parameter controlling the overall elastic response. In this region, especially at its lateral peripheries, variations of calculated tensile stresses are up to 2.5 MPa. Such amplitudes due to mass unloading have been shown to promote fracture initiation and eventual magma propagation (Andrew and Gudmundsson, 2007). In this context, stress changes after El Hierro's latest flank collapse appear more than sufficient to have caused perturbations in eruptive activity.

2.4.1. Comparison to other volcanic systems

Evidence of landslide-related perturbations in the magmatic and eruptive regimes has been reported from both stratovolcanoes and intraplate basaltic shields. At Mount St. Helens, for example, past lateral collapses are thought to have provoked a return to more mafic magma compositions (Pinel and Jaupart, 2000). Similarly, erupted magmas at Bezymianny volcano, Kamchatka, Russia, are gradually becoming more mafic since its catastrophic sector collapse in 1956 (Izbekov et al., 2001). Parinacota volcano, Northern Chile, has seen increased magma recharge rates, lesser degrees of fractionation, as well as a shift of the magma chamber to shallower levels after a late-Pleistocene sector collapse (Ginibre and Wörner, 2007).

Regarding ocean island volcanoes, Lipman et al. (1991) suggested that the lateral collapse associated with the formation of the southwest Hawaii slide complex on Mauna Loa volcano might have resulted in sudden, large phreato-magmatic eruptions from the landslide headwall. Presley et al. (1997) showed that Waianae volcano, on Oahu, erupted less differentiated magmas after a mass-wasting event some 6,100 km³ in volume. These authors proposed that, in addition to disturbing magma plumbing, the huge Waianae slump might have affected magma genesis in the mantle, in agreement with trace element chemistry. Moreover, Hildenbrand et al. (2004) claimed that eruptive rates immediately after a collapse episode on the northern flank of Tahiti-Nui Island, French Polynesia, were 2-5 times higher than during the volcano's initial shield phase and later activity. Temporal changes in lava chemistry appear to correlate with this landslide and were interpreted as related to increased partial melting in the mantle due to collapse-induced decompression.

To test the general applicability of the El Hierro results, we applied our modeling approach to simulate the effects of lateral collapse at other volcanic edifices (Fig. 2.4). Overall, decompression amplitude depends on the volume of the collapsed sector; however, the ratio between the initial and the final load as well as the radius of the initial edifice control rapid or slow decay of the decompression effect. Therefore, mass-wasting events that occur at different volcano types and that have volumes differing by orders of magnitude may induce similar pressure changes at depth. For example, the flank collapses at the Teno massif, Tenerife, Canary Islands, would have caused pressure changes in the lithosphere similar to those calculated for the mass-wasting event at Paríacota volcano, Chile, and at Mount St. Helens in 1980 (respectively 50 km³, 6 km³ and 2.5 km³, details are in the GSA Data Repository, Table DR2).

However, despite available geochemical data in agreement with potential landslide-induced increases in melt fractions at Hawaii (Presley et al., 1997) and Tahiti-Nui (Hildenbrand et al., 2004), our modeling results imply very low decompression values at depths relevant to mantle melting, suggesting that an effect on melt production is unlikely (i.e. \ll 0.5 MPa at ~80 km depth beneath El Hierro, see also GSA data repository, Section 5).

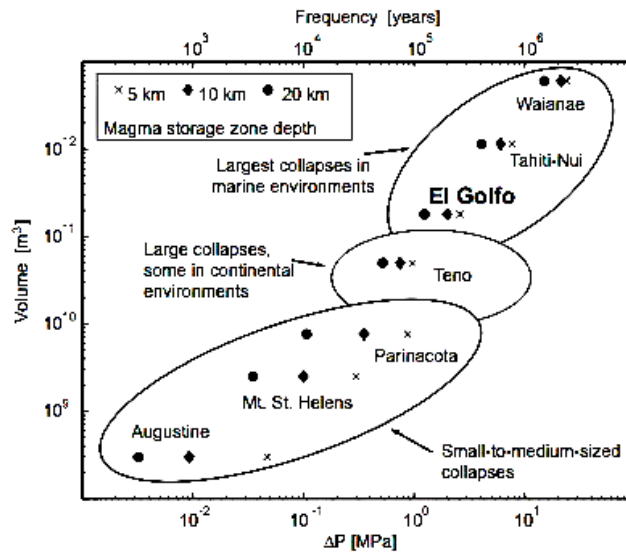


Figure 2.4: Landslide-induced decompression calculated for various volcanic systems. Log-scale axes show decompression (bottom x-axis), recurrence time (top x-axis, from McGuire, 1996) and flank collapse volume (y-axis). Decompression is calculated assuming a mechanically softer reservoir at three different depths beneath the edifices: 5 km (cross); 10 km (full diamond); 20 km (full circle). See text for details.

2.4.2. A conceptual model for magma remobilization after flank collapse

The load of a volcanic edifice acts as “a density filter” on the magmatic system (Pinel and Jaupart, 2000), i.e. the eruption of mafic, high-density magmas is hindered, and that of SiO₂-rich, low-density magmas promoted, as a volcano grows in size. After flank collapse, however, the volcanic load above magma chambers and conduits is displaced and reduced, which should itself help to widen the density window of eruptible magmas. In addition, if magmas are volatile-oversaturated at depth, which is the case for mafic alkaline ocean island magmas stored in the upper mantle (such as those of El Hierro, Hansteen et al., 1998; Stroncik et al., 2008), decompression is likely to enhance homogeneous bubble growth and nucleation. Gas expansion, and the resulting increase in magma chamber pressure and effective decrease in magma density, ought to facilitate magma propagation and ascent and, finally, further increases the probability of eruption of denser, more primitive, and crystal-rich magmas like ankaramites.

Furthermore, our modeling results show that a volcano flank collapse will induce relatively high-pressure gradients within magma reservoirs at depth

(Fig. 3a-b). By comparison, an El Golfo-sized landslide produces differential pressures, between the top and bottom of El Hierro's magmatic system that are on the same order of magnitude as those caused by large earthquakes, which have been shown to trigger subsurface fluid migration (Manga and Brodsky, 2006). Such fluid migration is thus also expected after flank collapse and will follow upward trajectories within a magma plumbing system, as defined by the super-imposed gradients (vectors in Fig. 3b). This process will promote the remobilization of magma batches stored at various levels and will bring fractional crystallization to a temporal halt. Magma mixing has long been recognized as an important eruption triggering mechanism (Anderson, 1976); however, the dynamic processes giving rise to magma mixing at depth are still debated. For volcanoes that suffer flank collapse, we suggest that pressure gradients generated by surface unloading are capable to induce instability into magmatic systems, thereby causing mixing of magmas, aggregation of their crystal populations, as well as their ascent and eruption (Nakagawa et al., 2002).

In summary, field and petrological evidence as well as the realistic numerical models presented here strongly suggest a cause-and-effect relationship between a large-scale flank collapse – the El Golfo landslide – and the increased eruptive proportions of dense, crystal-rich and mafic magmas at El Hierro Island. Landslide-induced disturbances in the state of stress of a volcano's magmatic system retain relatively large magnitudes down to important depths (e.g. upper mantle at El Hierro) and are likely to drastically alter storage, transport, mixing, differentiation and degassing of magma batches. These results provide a basis for thus far unexplained changes in the eruptive and geochemical regimes at volcanoes that have experienced large-scale destructive events.

Chapter 3

Effects of mechanical layering on volcano deformation[†]

Andrea Manconi ⁽¹⁾, Thomas R. Walter ⁽¹⁾, Falk Amelung ⁽²⁾

(1) GFZ German Research Centre for Geoscience, Potsdam, Germany; (2) Department of Marine Geology and Geophysics, RSMAS, University of Miami, USA

ABSTRACT

The migration and accumulation of magma beneath volcanoes often causes surface displacements that can be measured by geodetic techniques. Usually, deformation signals are explained using models with uniform mechanical properties. In this paper, we study surface displacements due to magma chamber inflation, using heterogeneous finite element models. We first present a systematic analysis of the influence of mechanical layering, showing that the stiffness contrast significantly affects the entity and the pattern of vertical and radial displacements. Second, as an example we apply the models to interpret ground displacements at Darwin volcano (Galápagos Islands) as revealed by InSAR data in the period 1992-1998. The considered

[†] **Author contributions:** A.M. carried out the finite element modeling, under the supervision of T.R.W. All the authors contributed to the hypotheses and the interpretations presented. Writing and illustrating was done by A.M., with the cooperation of all authors. This paper has been published in 2007 by the *Geophysical Journal International*.

models suggest that geodetic data interpreted using homogeneous models leads to underestimation of the source depth and volume change. Thus, we propose correction factors for the source parameters estimated by homogeneous models, in order to consider a range of variation due to mechanical layering as analyzed in this study. The effect of the mechanical heterogeneities affects the correct understanding of geodetic data and also influences the evaluation of a volcanic hazard potential.

3.1. INTRODUCTION

Studying the amount and pattern of surface deformation on volcanoes allows us to locate magma intrusions and to estimate the geometry and volume change of magma bodies (Dzurisin, 2006 and references therein). The spatial and temporal accuracy of geodetic techniques has increased significantly in recent years, as has the evaluation of the source of deformation in quantitative models (Jónsson, 1999; Amelung et al., 2000; Pritchard, 2004; Yun et al., 2006). Yet, most of the modeling attempts make use of simplified analytic solutions, for instance considering a point source in an isotropic elastic half-space (Mogi, 1958). Such a first order solution is still considered a fast and adequate way to analyze surface deformations due to magma intrusions (Dzurisin, 2006). However, volcanoes are mechanically heterogeneous and layered, which affects magma propagation, associated stress field and also surface deformation (Gudmundsson, 2006 and references therein). For example, a succession of thin sub-horizontal layers with different mechanical properties is common in basaltic volcanoes, as a result of alternating pyroclastic, effusive and erosive activity (Fig. 3.1). Laboratory measurements show that basaltic materials have values of the Young's modulus (E) between 10-100 GPa, whereas pyroclastic and sedimentary rocks commonly have values of 1-10 GPa or even less (Goodman, 1989; Bell, 2000). This implies that volcanoes are formed by piles of layers with a contrast of the Young's modulus of 1-2 orders of magnitude. The effect of the mechanical properties on distribution and entity of stress and

strain has thus been the subject of intense scientific debates. For instance, Savage (1987) inverted surface deformation data to obtain slip distribution on a vertical strike-slip fault, comparing layered models with homogeneous models, concluding that the effects of material properties could be important

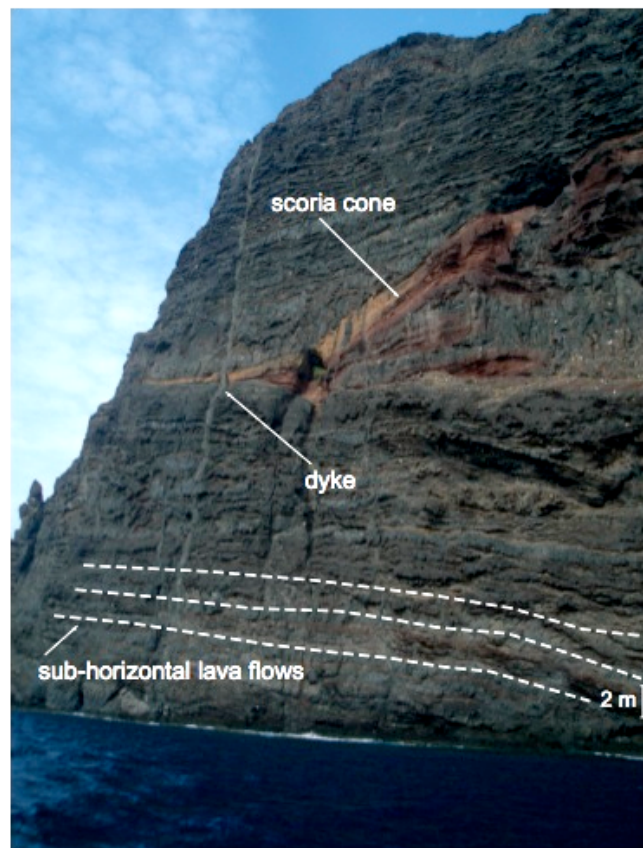


Figure 3.1: Example of layering in volcanic areas. Sub-horizontal shield basalt lava flows (black dashed line) and pyroclastic deposits (reddish). Gran Canaria (Canary Islands).

only for inversions with high spatial resolution. Roth (1993) studied deformations in a layered crust, emphasizing the effect of a soft material on the surface displacement field. Du (1997) studied geodetic data collected before and after the 1989 south Kilauea earthquake (Hawaii) and concluded that material heterogeneities could cause an underestimation of the earthquake source depth and an overestimation of the seismic moment. However, using the same model setup, Hooper et al. (2000) reconciled

seismic and geodetic models of the same case-study, showing that mechanical heterogeneities do not have as great an influence. Cattin et al. (1999) studied the influence of a superficial layer overlaying a half-space, explaining the effect of mechanical contrast on the estimation of fault depth. Rivalta et al. (2002) propose analytical solutions for edge dislocation in a layered medium, concluding that stress and displacement fields change significantly in the presence of discontinuities of the elastic parameters. Gudmundsson and Loetveit (2005) showed that mechanical layering influences -or even controls- emplacement of dykes in rift zones.

In the following study, we present systematic tests that will help to understand the influence of layered materials on the surface deformation process during volcano inflation. Then, we apply these models to Darwin volcano (Galápagos Islands), which was continuously inflating during the period 1992-1998 (Amelung et al., 2000).

3.2. MODELING

3.2.1. Method and setup

We use the commercial code Abaqus version 6.5 (HKS Inc., available at <http://www.hks.com>) to construct finite element (FE) models (Fig. 3.2). We begin with the comparison of homogeneous models with heterogeneous layered models. We consider an axisymmetric geometry, 80 km long in the radial, r direction and 100 km in the vertical, z , downward direction. The mesh is finer in the upper part of the model to obtain accurate results of surface deformation (Zienkiewicz, 1989; Fagan, 1992). As loading conditions we assume a volume change (ΔV) of a small finite spherical source (radius $a=0.1$ km) at depth, hereafter referred to as the magma chamber. As boundary conditions we assume zero normal strains at the right bound and at the bottom of the model. To validate our numerical solutions, the results of the models performed in a homogeneous medium are compared to Mogi's analytical model (Mogi, 1958), whereas convergence tests were performed for the heterogeneous models. Results of the simulations are presented in the

form of vertical (U_z) and radial (U_r) displacements, against the radial distance from the source. If not otherwise specified, displacements are normalized by the maximum vertical displacement of the homogeneous solution ($U_z/U_{z_{\max}}$), whereas radial distances r are normalized by the magma chamber depth d (r/d).

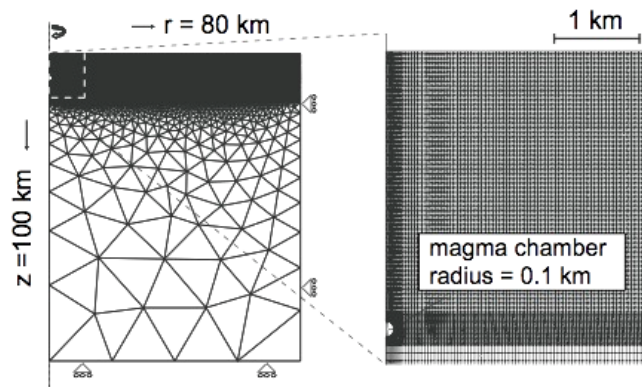


Figure 3.2: Geometry of the axisymmetric finite element models used in this study. Left: Mesh and boundary conditions (“rollers” indicate zero normal strains). Right: Detail of the mesh in the upper part of the model. The volume change is applied to a spherical magma chamber. In layered models, we considered within every layer a resolution of 800 nodal points in the radial, r , direction and 5 in the vertical, z , direction. The density of nodal points in the radial direction decreases gradually.

3.2.2.1. Homogeneous models

For the homogeneous model (H), we assume a Young’s modulus of 50GPa in the whole domain and a Poisson’s ratio of 0.25, i.e. typical laboratory values for basaltic material (Goodman, 1989; Bell, 2000). Inflation of the magma chamber at depth causes a vertical and radial displacement of the surface. Figure 3.3 shows that the homogeneous FE model agrees with the displacements predicted by Mogi analytical solution, confirming the reliability of our mesh and boundary conditions.

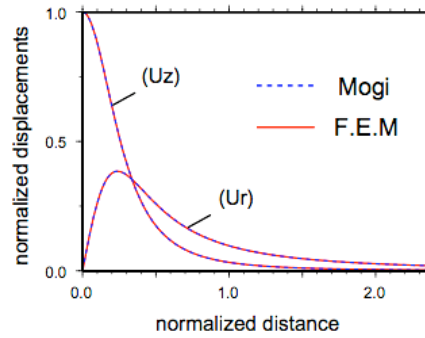


Figure 3.3: Model comparison of radial (U_r) and vertical (U_z) displacements between Mogi's analytical solution (blue dashed line) and our homogeneous finite element model (red line). The agreement suggests that the setup of our model is correct.

3.2.2.2. Heterogeneous models: effect of one layer above the homogeneous half-space

We now introduce mechanical heterogeneities in the FE models. First, we divide the models into an upper part (U) and a lower part (L) (Fig. 3.4a, step 1). This allows us to test how surface displacements differ for various Young's modulus of part L and part U, results of which are shown in figure 3.5. When part U is softer than part L ($E_U < E_L$), maximum vertical displacements and radial displacements are amplified with respect to the homogeneous model ($E_U = E_L$). When part U is stiffer than part L ($E_U > E_L$), our models predict smaller vertical and radial maximum displacements than the homogeneous model. In both cases, the vertical surface deformations are affected most directly above the source, whereas radial displacements are affected even at larger distance.

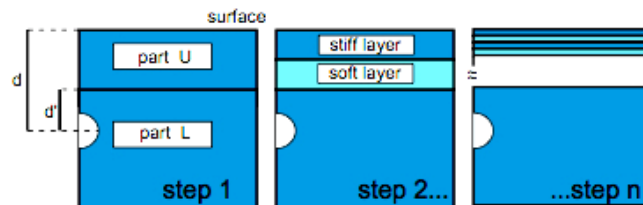


Figure 3.4: Multi-layered heterogeneous models. Scheme used to study the effect of mechanical layering. At step 1 we divide the model into an upper part U and a lower part L. The inflating magma chamber is embedded in the homogeneous part L at depth d from the surface and d' from the layered part U. Further layering is introduced in part U. At each subsequent step, we increase the number of layers in the part U while decreasing their thickness. We keep the same alternation scheme ("stiff-soft", stiff material at the surface) and also consider the opposite alternation scheme ("soft-stiff", soft material at the surface).

3.2.2.3. Heterogeneous models: effect of the number of layers

We used the above-described models, but consider a larger number of layers in the part U. We introduced two layers with the same thickness, layer “stiff” and layer “soft” (Fig. 3.4, step 2). We reproduced the model in several steps, at each step increasing the number of layers “stiff” and “soft” in the part U (Fig. 3.4, step 3 to n), i.e. decreasing their thickness. Within these steps we maintain the alternation scheme (“stiff-soft”, stiff material at the surface) but also consider the opposite contrast scheme (“soft-stiff”, soft material at the

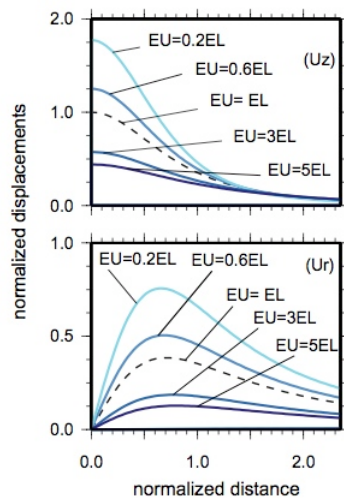


Figure 3.5: Influence of one layer overlying the homogeneous half-space on vertical (U_z) and horizontal (U_r) displacements (step 1, see figure 3.4). If the upper layer is stiffer than the half-space surface displacements decrease. On the contrary, if the upper layer is softer than the half-space surface displacements are amplified.

surface). We performed these steps for different magma chamber depths and for different mechanical contrasts (table 3.1), and compared the results with the homogeneous model H. Since all the tests yielded comparable results, here we show those of model A for a magma chamber depth of 3.5 km for simplicity (Fig. 3.6). Mechanical layering amplifies the amount of maximum U_z by more than 100%. Radial displacements are less affected in amplitude, but we note that in the layered models the location of maximum displacement is shifted closer to the source center. We find that for more than 20-layers, similar results are yielded in terms of both U_r and U_z . Small differences between “stiff-soft” and “soft-stiff” are related to local effects of the last layer

close to the source and first layer at the free surface. The root mean square (RMS) of the total surface displacements shows that U_z and U_r remain constant when 20 or more layers are considered. As illustrated in figure 3.7, this is the case for various magma chamber depths and contrast schemes.

3.2.2.4. Heterogeneous models: effect of the mechanical contrast

The differences in displacements revealed by the previous simulations might be related (a) to the change of the average Young's modulus E_{Av} , where the E_{Av} is the mean of the moduli considered in part U ($E_{Av} = \frac{1}{2} [E_{stiff} + E_{soft}]$), or (b) to the change of the mechanical contrast between layers "stiff" and "soft". However, as shown in figure 3.8, the displacements U_z and U_r may differ even if E_{Av} is the same (e.g. models B and C). This implies that the contrast between the layers is controlling the amount of displacements at the surface. In the following section we will apply the layered models to study the source parameter of an inflating volcano on the Galápagos Islands.

Models	Part U		Part L (GPa)
	Layers stiff (GPa)	Layers soft (GPa)	
Model H	50	50	50
Model A	50	10	50
Model B	70	30	50
Model C	90	10	50
Model D	50	10	100

Table 3.1: Mechanical setups analyzed in this study. The models considered in this study are shown in the first column. Model (H) is homogeneous; models A-D are heterogeneous. In the other columns are shown the Young's modulus values for the different parts of the models, respectively part U, tailed in stiff layers (column 2) and soft layers (column 3), and part L (column 4). See text for details.

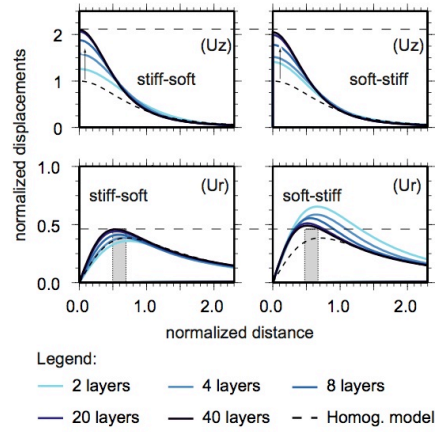


Figure 3.6: Influence of number and/or thickness of layers on part U (step 2-n, see figure 3.4). Here are shown the results for magma chamber at 3.5 km depth (model A setup). The upper two graphs show vertical displacement U_z , the lower two graphs show radial displacement U_r , the left column is with stiff layer at the surface, the right column with soft layer at the surface. Vertical and horizontal surface displacements in layered models are amplified in respect with the homogeneous half-space (dashed line). Note that displacements of the models on the left (“stiff-soft” scheme) and the models on the right (“soft-stiff” scheme) converge if more layers are considered.

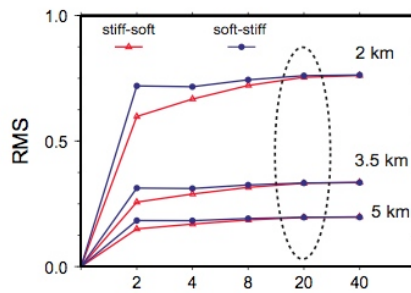


Figure 3.7: Root mean square (RMS) of total displacements calculated for three different magma chamber depths (2, 3.5, 5 km) and contrast orders (“stiff-soft” and “soft-stiff”) considered in this study. After 20-layers (dashed ellipse) the displacements are only slightly affected by a further increase of the number of the layers.

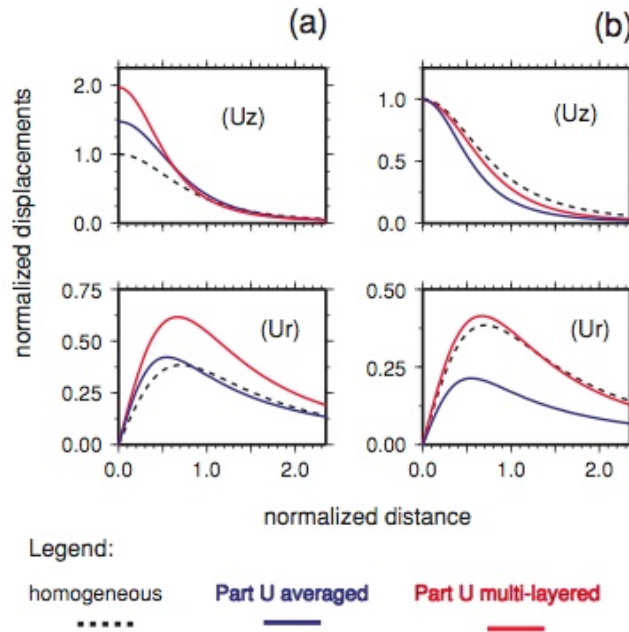


Figure 3.8: Effects of the mechanical contrast between layers in part U. Model H (dashed line) is homogeneous. The other models are made up by 20-layers. Model B and C have the same average Young's modulus E_{Av} . a) Displacements are normalized by U_{zmax} of the model H, showing that the contrast between layers affects the absolute values of vertical (U_z) and horizontal (U_r) surface displacements; b) Displacements of each model are now normalized by their own U_{zmax} .

3.3. APPLICATION TO DARWIN VOLCANO

3.3.1. Surface deformation on the Galápagos Islands

The Galápagos archipelago is a volcanic hot-spot located 1,000 km west of Ecuador. The youngest and most active volcanoes are located on Isabela and Fernandina Islands, with about 60 reported eruptions since the early 1800s (Simkin, 1994) (Fig. 3.9). These basaltic islands are characterized by flanks gently sloping and large summit calderas (McBirney, 1969; Geist et al., 1994; Munro and Rowland, 1996). The volcanoes' activity has recently been studied by measurements of surface displacements using space-based geodetic techniques (GPS and InSAR) (Jónsson, 1999; Amelung et al., 2000; Rowland et al., 2003; Jónsson et al., 2005; Geist et al., 2006; Yun et al., 2006). Most of the Isabela and Fernandina calderas have been actively deforming since 1992, as shown by Amelung et al. (2000). In their study, an uplift of about 20 cm line-of-sight (LOS) was revealed at Darwin volcano in the period 1992-

1998. Because the pattern of the ground displacements was near-radial symmetric, a Mogi point source embedded in a homogeneous half-space was used to estimate the depth and the volume change of the magma chamber. Using this simplified model, the best-fit solution suggests an inflation source in the center of the caldera at 2.7 km depth and a volume change of $5.8 \times 10^6 \text{ m}^3$. The following section shows that consideration of material heterogeneity may largely affect this interpretation.

3.3.2. Darwin volcano heterogeneous models

Displacements predicted by the heterogeneous models (models A, B, C and D) are compared with these predicted by the homogeneous model H. We performed a linear inversion of the volume change and assume as magma chamber depths values between 2 and 5 km, which are in agreement with the depth range of the level of neutral buoyancy of magmas in basaltic volcanoes (Ryan, 1988). In comparing the models to the observed data, we define a section a-a', which is chosen parallel to the looking angle of the satellite (see Fig. 10). The location and volume of the magma chamber are constrained by the maximum displacement in the section a-a'. Since our FE model is radial symmetric, we first select the best-fitting models along a northwest-southeast

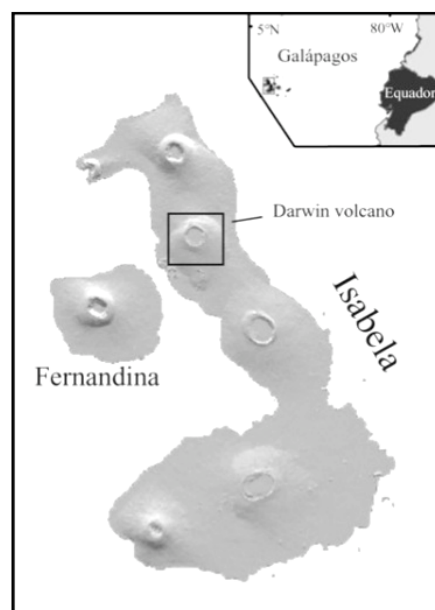


Figure 3.9: Geographic overview and shaded relief map of the Galápagos Islands. The studied caldera area on Darwin volcano is indicated with a black box.

section a-a' and generate synthetic interferograms by sweeping the results along 360°. All simulated mechanical setups show reasonably good fits of the displacement signal. However, the depth of the source predicted by heterogeneous models (see table 3.2) differs by up to 1.5 km (model H = 2.7 km, whereas model C = 4.25 km). Model A and D, both of which predict the source at 3.75 km depth, show the best agreement with the observed data in the inner part of the caldera. In those models, consideration of an increase of the Young's modulus with depth (see also Du, 1997; Okubo et al., 1997; Hooper et al., 2002) is affecting the volume change, although the magma chamber depth may remain the same. Moreover, we note that the change in volume predicted by heterogeneous models is generally larger than that of the homogeneous model (model H = $5.8 \times 10^6 \text{ m}^3$; model A = $5.98 \times 10^6 \text{ m}^3$; model B = $7.74 \times 10^6 \text{ m}^3$; model C = $7.14 \times 10^6 \text{ m}^3$; model D, $4.93 \times 10^6 \text{ m}^3$). This example from the Darwin volcano shows that both estimation of the source depth and volume change increase if a mechanical layering is considered.

Models	d (km)	k_d	ΔV ($\times 10^6 \text{ m}^3$)	k_v
Model H	2.7	1	5.8	1
Model A	3.75	1.38	5.98	1.03
Model B	3.25	1.2	7.74	1.33
Model C	4.25	1.57	7.14	1.23
Model D	3.75	1.38	4.93	0.85

Table 3.2: Magma chamber depth and volume change at Darwin volcano. The models considered in this study are shown in the first column. Model (H) is homogeneous; models A-D are heterogeneous. Columns 2-3 show the predicted magma chamber depths (d) and their correction factors (k_d). Columns 4-5 show the predicted volume change (ΔV) and their correction factors (k_v). See text for details.

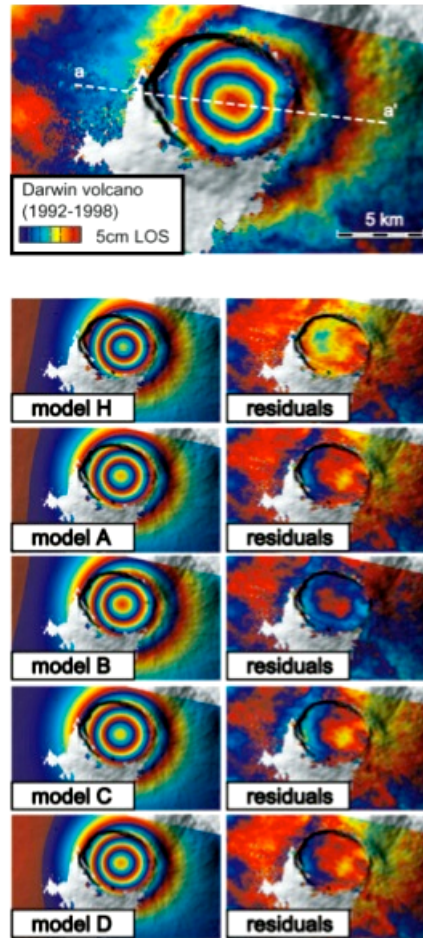


Figure 3.10: InSAR line-of-sight (LOS) surface displacements at Darwin volcano during 1992-1998. (Top panel) LOS displacements towards ERS-1 and ERS-2 satellites. The images are from track 140, descending orbit. Baseline is 85 m. Azimuth looking angle of the satellites is $\sim 283^\circ$, whereas incidence angle is $\sim 23^\circ$. Section a-a' is parallel to the looking angle of the satellite. Each cycle colour represents 5 cm of LOS displacement. See also Amelung et al. (2000); (down panel) (left column) Synthetic LOS displacements predicted by the five different models considered in this study, with the homogeneous model H, and the heterogeneous layered models A-D; (right column) Residual analysis show that all layered models yield very good results in reproducing the observed surface displacement.

3.4. DISCUSSION

We studied surface deformation due to magma intrusions using layered heterogeneous finite element models. Systematic tests suggest that we do not have to consider all the layers as we observe in nature, and that depth and volume changes of inflating magma bodies are different if calculated in layered heterogeneous models.

3.4.1. Influence of the layering on displacement field

It is common in basaltic volcanoes to find a succession of thin sub-horizontal layers, often with alternating mechanical properties. Considering a basaltic volcano made up by a pile of 5 m thick lava flows overlaying a magma chamber at 5 km depth would mean that we have to consider 1000 layers. In our simulations, however, after the value of 20-layers (which corresponds to a layer thickness of 90-240 m for source depths between 2 km and 5 km), displacements are only slightly affected by a further increase of the number of layers, independently on the considered source depth. Therefore, we chose 20-layers to approximate Darwin volcano heterogeneous models.

3.4.2. Implications for Darwin volcano source parameters

We studied the uplift revealed at Darwin volcano, yielding within the caldera basin to good agreement between data and layered FE models. However, a slight misfit on the caldera rims can still be observed. This misfit could be due to a more complex shape of the magma body, due to topographic or atmospheric effects, due to other material heterogeneities or also due to ring fault dislocation. The mechanical layering affects the depth of the source and also its volume change (model B and C). This implies that models based on the assumption of homogeneity cannot be used for quantitative determination of the source parameters. To overcome this problem we may introduce correction factors (k_d for the depth and k_v , for the volume change, see table 2), to adjust the source parameters estimated in homogeneous models and discuss their variations due to heterogeneous mechanical setups as used in this study. Because the magma chamber depth determined through homogeneous half-space models is underestimated, a depth correction factor k_d generally larger than 1 is considered for models herein. This is also in agreement with the results of other authors studying fault dislocation in layered media (e.g. Roth (1993), Du et al. (1997), Cattin et al. (1999) and Rivalta et al. (2002)). The trend for the volume change is variable, thus k_v may be larger or smaller than 1. In summary, in order for the considered models herein to interpret ground uplift at Darwin volcano, k_d varies between 1.2-1.57, whereas k_v between 0.85-1.33.

3.4.3. Validation and limitations of the models

Although we use heterogeneous FE models, a number of simplifications were necessary. We considered a spherical source of 0.1 km radius, which is only a first order approximation for a real magma chamber. The effect of larger finite spherical sources was studied in homogeneous models by Mc Tigue (1987), showing that the surface uplift is controlled by the ratio of radius to the depth, so that $\epsilon = a/d$. Point source and finite sources accordingly achieve similar surface displacements as long as $\epsilon < 1/3$, whereas for $\epsilon > 1/3$ the point source tend to underestimate the source depth (Dietrich et al., 1975; Mc Tigue, 1987). In layered models a similar limitation has to be considered also for the distance d' between the source and layers of part U, so that $\epsilon' = a/d'$. In the herein presented 20-layered models, we achieve very similar results (differences less than 1%) when considering the “stiff-soft” and “soft-stiff” configurations (see fig. 6 and 7), where $0.5 < \epsilon' < 0.22$. This small difference, however, might also be related to the effect of the first layer at the free surface. Thus, our estimation of Darwin volcano source parameters in layered models is constrained by the herein assumed geometry. This means that if we would consider a bigger source (e.g. $a = 1\text{km}$) the differences between the depth estimated in Amelung et al. (2000) and our results would be larger. Furthermore, consideration of more realistic non-spherical shapes of a magma chamber may also affect the stress and displacement field as shown previously by other authors (e.g. Yang et al. 1988, Fialko et al. 2001, Gudmundsson 2006). We hence assume that layering affects the correct assessment of these bigger and more complex magma chamber sources as well.

In our models we neglect time dependent and anelastic behaviour around the magma chamber, which can further influence the surface displacement (Newman et al., 2006). Furthermore, we consider simple horizontal layers, with the same thickness and alternating mechanical properties, as a reasonable approximation only for very flat basaltic volcanoes. Vertical anisotropies (e.g. dikes or faults), dipping layers or otherwise weak contacts between layers may affect the symmetry of stress changes and may likewise lead to asymmetric ground displacement patterns (Gudmundsson, 2006). This means that complex deformation patterns may be a consequence of complex

material heterogeneities. Additionally, hydrothermal systems may alter the values of mechanical strength of the rocks, causing local stiffness variations as large as two orders of magnitude (Watters et al., 2000). The largest limitation of more realistic heterogeneous models is, however, that hardly any in situ data resolving mechanical contrasts on active volcanoes are available. The few laboratory measurements available resulted from using small-scale samples, and not representative for km-scale natural mechanisms. However, we point out that variation of stiffness contrasts in simple configurations can influence the estimation of source parameters, which is crucial not only for the correct interpretation of geodetic data, but also for the correct evaluation of a volcanic crisis. For example, an underestimation of the source volume change and depth could mislead the calculation of magma accumulation and ascent rates.

3.5. CONCLUSIONS

We performed systematic tests to understand the influence of mechanical layering in surface deformation studies. We applied our models to interpret the ground uplift revealed by InSAR data at Darwin volcano during 1992-1998.

In summary, our models of magma chamber inflation show that mechanical layering affects the pattern and the magnitude of ground deformation. Within our modeling assumptions, for flat basaltic volcanoes consideration of at least 20-layers geometry appears to provide a reliable prediction of the displacement field at the surface. Furthermore, this study shows that homogeneous models could underestimate the magma chamber depth and volume change. In a non-layered homogeneous model of Darwin volcano, the depth and volume change of the magma chamber are at $d=2.7$ km and $\Delta V=5.8 \times 10^6 \text{m}^3$ (Amelung et al. 2000), compared to the magma chamber depth variation between $3.25 < d < 4.25$ km, and magma chamber volume change $4.93 < \Delta V < 7.74 \times 10^6 \text{m}^3$ in our layered heterogeneous models.

Chapter 4

The source of ground deformation at Campi Flegrei caldera during the last 16-years: insights from Finite Element modeling and SBAS-DInSAR time series analysis[†]

Andrea Manconi ⁽¹⁾, Thomas R. Walter ⁽¹⁾, Mariarosaria Manzo ⁽²⁾, Giovanni Zeni ⁽²⁾, Pietro Tizzani ^(2, 3), Eugenio Sansosti ⁽²⁾ and Riccardo Lanari ⁽²⁾

(1) Dept. Physics of the Earth, GFZ German Research Centre for Geoscience, Potsdam, Germany; (2) Istituto per il Rilevamento Elettromagnetico dell'Ambiente, Consiglio Nazionale delle Ricerche, Napoli, Italy; (3) INGV-Osservatorio Vesuviano, Napoli, Italy.

ABSTRACT

Campi Flegrei caldera, located near the highly populated city of Naples, (Southern Italy), is characterized by long-term subsidence punctuated by fast uplift phases. Most of the first order interpretations of the measured ground deformation are still based on models that assume the lithosphere to behave as a homogeneous half-space. However, several geophysical investigations show the presence of vertical and lateral heterogeneities especially in the

[†] **Author contributions:** A.M. carried out the finite element, as well as the inverse source modeling. M.M., G.Z. and P.T. provided the 16-years InSAR time series of Campi Flegrei caldera. All the authors contributed to the hypotheses and the interpretations presented. Writing and illustrating was done by A.M., with the cooperation of all authors. The manuscript has been submitted to *Journal of Geophysical Research*.

shallow subsurface, which might have an effect on the interpretation of the surface displacements.

Here we use finite element models, constrained by a 3-D seismic tomography, to take into account a realistic distribution of mechanical heterogeneities. We demonstrate that at Campi Flegrei the assessment of the source location is independent on the consideration of 3-D heterogeneities, while the evaluation of its strength might be overestimated by as much as 35%. Due to the linear relationship between the source strength and the surface displacements, we propose a procedure to correct the values retrieved using standard homogeneous models for the 3-D heterogeneity effects. We apply this method to study the deformation source at Campi Flegrei caldera over the past sixteen years, analyzing the complete SBAS-DInSAR dataset. The results of our integrated study provide quantitative constraints for the evaluation of the volume and pressure changes at depth during the unrest phases at Campi Flegrei caldera, and have also some general implications for other volcanic areas, where a similar approach might be considered.

4.1. INTRODUCTION

Ground deformation in volcanic areas is the surface expression of deep-seated physical processes, which might be related to renewed magma emplacement or to changes within a pre-existing magmatic and/or a hydrothermal reservoir. The analysis of the surface displacement helps to understand the source at depth, such as the location, the shape, the volume/pressure changes, which are indispensable parameters for the assessment of a volcanic hazard potential (Dzurisin, 2006).

Campi Flegrei (CF) caldera, Southern Italy, alternates periods of slow ground subsidence with phases of rapid uplift. This behavior is monitored using ground-based (EDM, leveling) and space-based geodetic techniques (GPS, DInSAR). The analysis of the deformation signal is usually performed setting up inverse problems, which consider simple sources embedded in a homogeneous half-space. However, recent studies have shown that the

hypothesis of homogeneity in volcanic areas is an oversimplification that might lead to misinterpretations of the retrieved source parameters, especially of the source depth and strength (Trasatti et al., 2005; Crescentini et al., 2007; Manconi et al., 2007; Masterlark et al., 2007).

In this study, we use 3-D heterogeneous finite element models in order to include a realistic distribution of the mechanical properties of CF caldera. The aims of this work are: (i) to show the implications of the consideration of a oversimplified homogeneous model assumption for the interpretation of the deformation field at CF caldera and (ii) to propose a fast and reliable methodology to take into account the effects of mechanical heterogeneities in standard analyses of ground displacements at CF caldera.

After a brief introduction about CF caldera and its recent unrest history, the paper is organized as follows. We describe the construction of the 3-D heterogeneous finite element models, constraining the elastic mechanical properties by means of available seismic tomography information. Then, we detail the synthetic tests performed to assess the capability of simplified homogeneous models to attain a reliable solution when a more complex heterogeneity distribution is considered. The results show that the consideration of a realistic distribution of mechanical heterogeneities at CF caldera has major effects only on the estimation of the source strength. Hence, we propose a method that allows using the standard homogeneous models, but “corrected” for the 3-D heterogeneity effect. Finally, we apply this method to the analysis of the 16-year deformation time series at CF caldera. The latter has been measured by the application of an advanced Differential Synthetic Aperture Radar Interferometry (DInSAR) technique, referred to as Small BAseline Subset (SBAS) approach (Berardino et al., 2002), on a dataset of satellite images spanning from 1992 to 2008. Our analysis provides constraints for the understanding of the source evolution at CF caldera over the past 16-years, and several important constraints for future analysis of the surface displacements in this area.

1.1. CF caldera: recent unrest’s history

CF caldera (fig. 4.1) is a 12 km wide collapse structure formed by two major eruptions: the Campanian Ignimbrite and the Neapolitan Yellow Tuff (39 kyr

BP, VEI=7 and 15 kyr BP, VEI=6, respectively, Mastrolorenzo and Pappalardo, 2006). In the post-caldera phase, the activity in the area has been characterized by long-term subsidence punctuated by fast uplifts phases, with the latest eruptive event occurring in 1538 AD (Monte Nuovo eruption) after a ground inflation of several meters (Belluci et al., 2006). The most important recent uplift occurred between 1969-1971 and 1982-1984, when the city of Pozzuoli has been raised in total by about 3.5 m. The surface displacement has been accompanied by several earthquakes, which caused damages to the buildings and also the evacuation of 40,000 people (Bianco et al., 2004). Since 1985, the subsidence trend re-started, interrupted by uplifts of smaller amplitude in 1989, 1996, 2000 and 2004, again accompanied by seismic swarms (Troise et al., 2007).

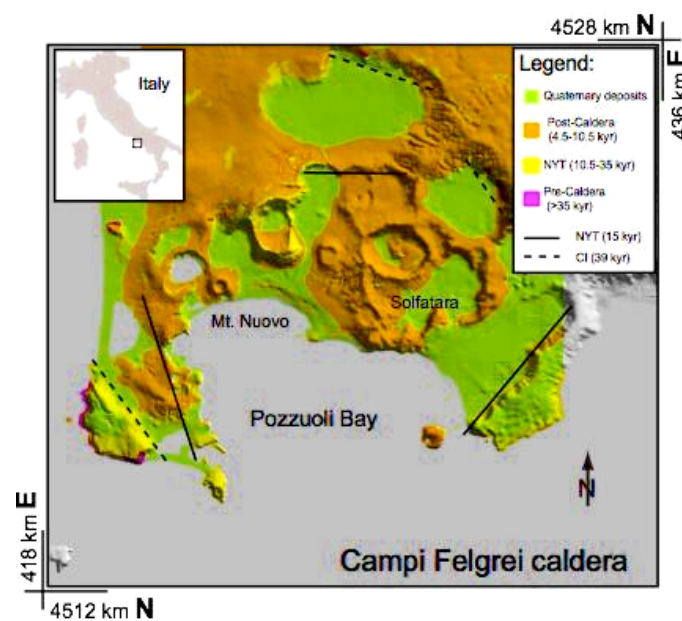


Figure 4.1: Sketch of the geological map superimposed on the Digital Elevation Model of the Campi Flegrei caldera. Mostly Quaternary soft materials and young volcanic deposits compose the inner caldera basin. Inferred ring faults caused by the Campanian Ignimbrite (CI) and the Neapolitan Yellow Tuff (NYT) caldera collapses are represented by solid and dashed black line, respectively.

The geodetic signal has been used by a number of authors in order to characterize the source responsible for the ground deformation at CF caldera. Most of the studies agree on a source located beneath the center of the caldera between 2.5 and 3.5 km depth. However, parameters as geometry, dimensions, strength and nature (magmatic, hydrothermal, and/or hybrid) of

the reservoir strongly depend in turn on the analyzed dataset and on the considered modeling assumptions. Several authors interpreted the ground deformation and seismic activity as related to pressure variations within the hydrothermal reservoir (De Natale et al., 2006). However, a comprehensive explanation of the long-term as well as the short-term ground deformation pattern is currently matter of discussion (e.g. Gottsmann et al., 2006; Bodnar et al., 2007; Amoruso et al., 2008). More than 3 million people live in the surrounding of CF caldera, considering the city of Naples and sub-urban area, making this volcanic region one of the most hazardous on Earth (De Natale et al., 2006). Therefore, a fast, precise and reliable assessment of the source parameters is important not only for the general understanding of the geodetic signal related to volcanic processes, but also crucial for volcanic hazard assessment in such a densely populated area.

The geophysical information relative to the subsurface of CF caldera provides important constraints for the modeling and the interpretation of geodetic data (De Natale et al., 2006 and references therein). In this framework, seismic tomography has been shown to be an important tool for crustal structure mapping. For example, Chiarabba and Moretti, (2006) proposed a 3-D velocity model after a tomographic study that included the analysis of active and passive seismic data. Their study shows the mechanical contrast between the external rim of the caldera, characterized by higher V_p velocities hence stiffer material, and the internal caldera basin structure, composed by softer sediments and incoherent materials. In the following, we will use 3-D information derived from seismic tomography in order to constrain the elastic mechanical properties of 3-D finite element models of CF caldera.

4.2. FINITE ELEMENT MODELS OF CF CALDERA

Finite element (FE) models here presented to investigate CF caldera's ground deformation have been constructed using the Structural Mechanics module of the Comsol Multiphysics™ package. The models are three dimensional,

200x200x100 km in xyz direction, discretized into ~17,000 tetrahedral elements, with higher resolution in their central part (fig. 4.2). The performance of the discretization has been verified through a convergence test (Fagan, 1992), finding that a higher resolution would affect the surface displacements of values smaller than accuracies achievable with standard geodetic technique (< 0.1 mm). Due to the almost flat surface of CF caldera, the topography is assumed to have minor influence on the displacement field (Cayol and Cornet, 1998), hence is herein not considered. Zero normal strains on lateral extremities and at the bottom of the models (“rollers” condition) have been assumed to avoid any boundary effect.

The 3-D mechanical setup of the heterogeneous FE model (hereafter referred to as 3DHET) is obtained converting seismic velocities, from the tomographic study of Chiarabba and Moretti, (2006), to the relative elastic parameters using the empirical relations proposed by Brocher (2005). The resulting values of shear moduli, Young’s moduli and Poisson’s ratios in the first 4 km of the subsurface at CF caldera are in the range of 2-14 GPa, 5-35 GPa and 0.2-0.4, respectively (fig. 4.2 b-c).

The displacements are calculated at the surface on a uniform grid with spatial resolution of 500m. Since our analysis focuses on the source assessment using as geodetic signal the SBAS-DInSAR dataset (see section 4.3), also for the synthetic tests we projected the surface displacements on the satellite’s ascending and the descending viewing geometries (line-of-sight, LOS), and retained only the areas visible in both (hereafter referred to as SBAS-stations). A detailed discussion about the model parameters, approximations and assumptions follows in section 4.4.

4.2.1. FE Synthetic tests

In order to evaluate the effects of 3-D distribution of mechanical properties, we applied the following approach. We simulated a positive volume change (ΔV) of about 1 Mm^3 within a small spherical source located beneath the center of the 3DHET model at 3 km depth. The calculated synthetic surface deformation is added with random noise, in the order of the accuracies of the SBAS-DInSAR technique (± 0.5 cm, Casu et al., 2006). We inverted the

obtained synthetic displacements using a procedure based on a Genetic Algorithm (GA, Holland, 1975), which is standard and efficient tool in geodetic

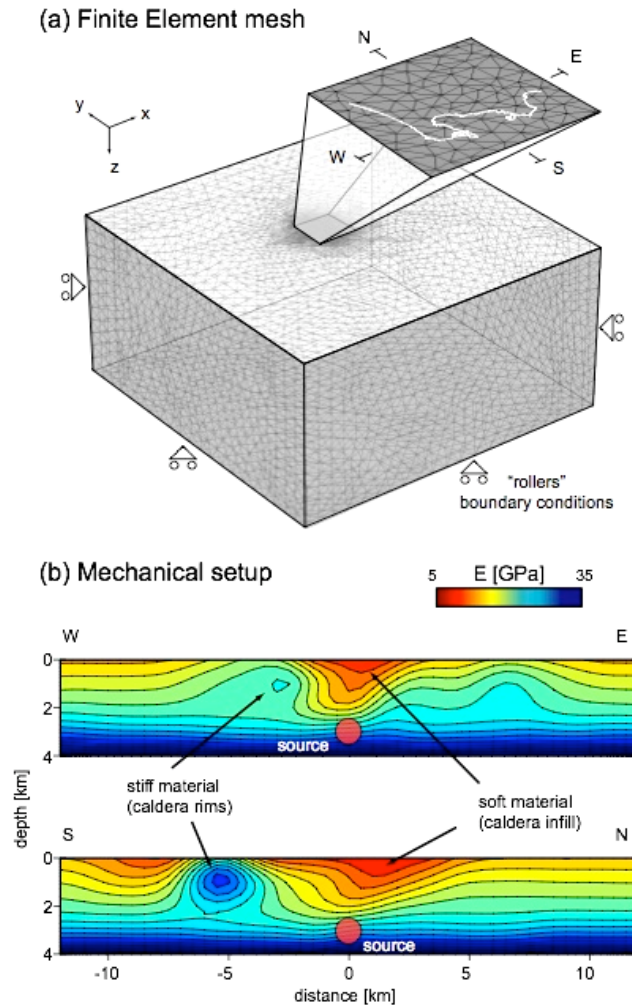


Figure 4.2: Setup of the 3-D finite element models. (a) Mesh and boundary conditions; (b-c) Mechanical configuration represented by the distribution of the Young's modulus (E) along two profiles, West-East and South-North, respectively. The modeled spherical source is located in the middle of the caldera at 3 km depth (see text for more details).

optimization problems (Nunnari et al., 2005; Shirzaei and Walter, in press). We minimized the difference between surface displacements caused by the dilatation of a point source embedded in a homogeneous half-space (Mogi, 1958) and the synthetic data assuming as cost function the L2 norm. Confidence interval for the parameters is inferred considering the range of values for the models that fall within 10% of the minimum cost (Picozzi et al., 2005).

The results of the synthetic tests show very good agreement between the modeled surface deformation, found after the optimization procedure, and the initial synthetic data (fig. 4.3). Moreover, the estimated values for easting, northing and depth of the source are in agreement with the imposed initial values (table 4.1). However, the inferred ΔV results up to 35% larger. This suggests that the assumption of homogeneous mechanical properties in the analysis of the geodetic at CF caldera, i.e. using the usual standard approach, does not affect the assessment of the source location, but might mislead its strength.

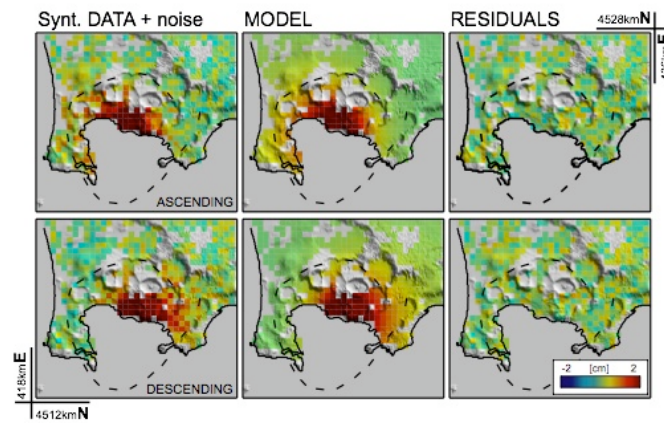


Figure 4.3: Synthetic tests. Deformation generated by a volume change on a small spherical source embedded on a 3-D heterogeneous, added with random noise and inverted assuming an isotropic point source embedded on a homogeneous half-space. Residual maps show the good agreement of the model with the synthetic data. See the text for more details.

East [km]		North [km]		Depth [km]		ΔV [Mm^3/yr]		rms [cm]
Min	Max	Min	Max	Min	Max	Min	Max	
426.4	426.9	4519.2	4519.5	2.8	3.1	1.15	1.35	0.3

Table 4.1: Range of parameters attained from the inversion of the synthetic displacements, generated within a 3-D heterogeneous finite element model (3DHET), assuming a homogeneous half-space instead, as usually done. The initial values, imposed in the 3DHET model, were $E=426.82$ km, $N=4519.3$ km, $depth=3$ km, and $\Delta V=1$ Mm^3 . While the source position is well constrained from the homogeneous assumption, the volume change is overestimated up to 35%.

4.2.2. “Correction” for the 3-D heterogeneity effects

In order to retrieve an accurate estimation also for ΔV using homogeneous models, we applied to the measured data a “correction” function defined as:

$$U_{corrected(x,y,0)} = U_{InSAR(x,y,0)} - \frac{K_{(x,y,0)} \cdot \max(U_{InSAR(x,y,0)})}{w} \quad (4.1)$$

where U_{InSAR} are the measured displacement at the surface, K and w are respectively a correction function and a weighting factor that depend on the 3-D mechanical heterogeneity distribution inside the CF caldera, and $U_{corrected}$ are the surface displacements “corrected” for the 3-D mechanical heterogeneities effects. The inversion of $U_{corrected}$, assuming as model a point source embedded in a homogeneous half-space (HHS), will retrieve source parameters similar as they were calculated in a fully 3-D heterogeneous medium consistent with the tomography velocity model (Chiarabba et al., 2006). Details about the determination of K and w , as well as the implications of the choice of an average HHS representative of the mechanical characteristics of CF caldera are referred to the Appendix. In the following, we use the “correction” function to interpret the real deformation field revealed at CF caldera over the past 16-years.

4.3. APPLICATION TO GROUND DEFORMATION MEASURED AT CF CALDERA

We applied the advanced DInSAR technique, referred to as Small BAseline Subset (SBAS) approach (Berardino et al., 2002), to a set of 165 ERS and 62 ENVISAT SAR data acquired between 1992 and 2008 on ascending (track 129, frame 809) and descending (track 36, frame 2781) orbits. Below, we first summarize the SBAS-DInSAR technique and the deformation field revealed at CF caldera. Secondly, we first inverted the surface displacements using a “standard” approach, and then applied the “correction” function to consider the effects of 3-D heterogeneity.

4.3.1. SBAS-DInSAR technique

The SBAS-DInSAR approach involves the selection of SAR image pairs to generate interferograms, which are characterized by a small temporal and spatial separation, and may include images acquired with different SAR sensors (Pepe et al., 2005). After a phase unwrapping procedure, the information available from the interferograms is inverted by using a Singular Value Decomposition (SVD) method. The latter process allows retrieving pixel-wise displacements relative to every acquisition date, providing a dense spatial and temporal resolution of the deformation field. The accuracy of the technique has been quantified to be ± 0.5 cm and ± 0.1 cm/yr for the measured ground displacements and velocities, respectively (Casu et al., 2006).

Figure 4.4 shows mean velocity maps of the ascending and descending information retrieved at CF caldera. Both images evidence an ongoing subsidence with an average velocity up to 3 cm/yr, which is the dominating trend of the last 16-years. However, the displacement time series show a non-linearity behavior (fig. 4 c-d), and provides details about of the evolution of two well-known recent uplift periods in 2000-2001 and 2004-2006 (Lanari et al., 2004; Trasatti et al., 2008).

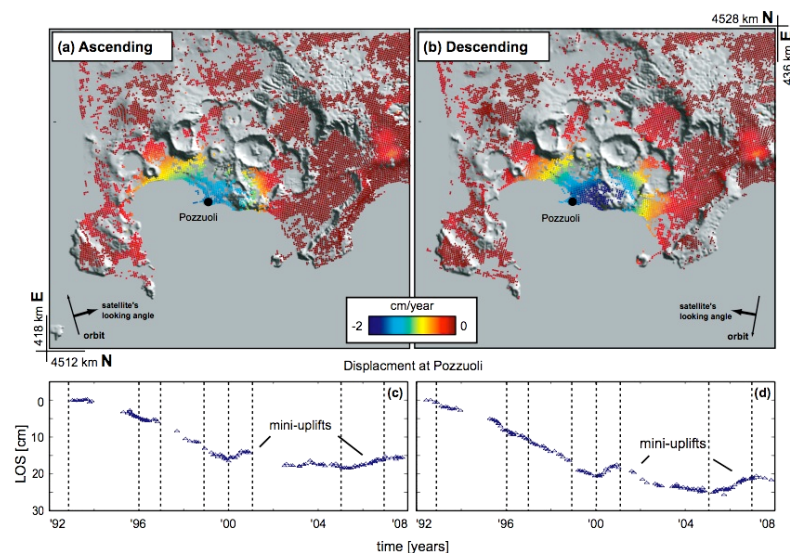


Figure 4.4: Mean deformation velocity maps superimposed on the Digital Elevation Model of the Campi Flegrei caldera. The values are computed by means of the SBAS-DInSAR technique on (a) ascending and (b) descending images acquired between 1992 and 2008. (c) and (d) show the time series of the deformation in Pozzuoli, a city located almost in the centre of the caldera system, clearly identifying the sub-linear subsidence trend (1992-2000) interrupted by two uplift phases in 2000-2001 and 2004-2006.

4.3.2. Source inversion

The time series has been analyzed considering two distinct procedures: (i) step-wise inversion of the cumulative displacements and (ii) inversion of stacks with a relatively large signal-to-noise ratio. For case (i), the full resolution dataset has been considered (90x90 meters), inverting the ascending and descending information separately. For case (ii), ascending and descending velocities calculated at the SBAS-stations (see section 2) have been jointly inverted. To achieve a reliable estimation of the source parameters, all inversions have been iterated at least 100 times, for a total of about 1 million of models evaluated for every acquisition date and data stack.

4.3.3. Results

The corrected SBAS-DInSAR data ($U_{\text{corrected}}$), the simulated models and residuals from the inversion of the data stacks are shown in figure 4.5, as best representative of the whole performed analysis. In general, the residuals verify a good agreement between the models and the measured data, with some anomalies that seem to be related more to localized mechanical heterogeneities or to remaining noise rather than to a different geometry of the source model. The source parameters retrieved from the optimization procedure are summarized in Table 4.2 and 4.3, and visualized in figure 4.6. Northing and Easting of the source remain stable during the whole period of observation. Moreover, the source depth is well constrained between 2.5 and 3.5 km. ΔV follows the subsidence and uplift phases, imaging the non-linearity of the behavior of the source at depth.

The application of the “correction” function to the measured data does not affect the estimations of the source location (Easting, Northing and depth) compared to the results previously obtained. However, the values of ΔV are remarkably smaller, as expected from the results of the previous synthetic tests (section 4.2). This result confirms the applicability of the proposed “correction” method to dataset of real measured data. Moreover, smaller ΔV involve a number of important implications for the assessment of source pressures at CF caldera.

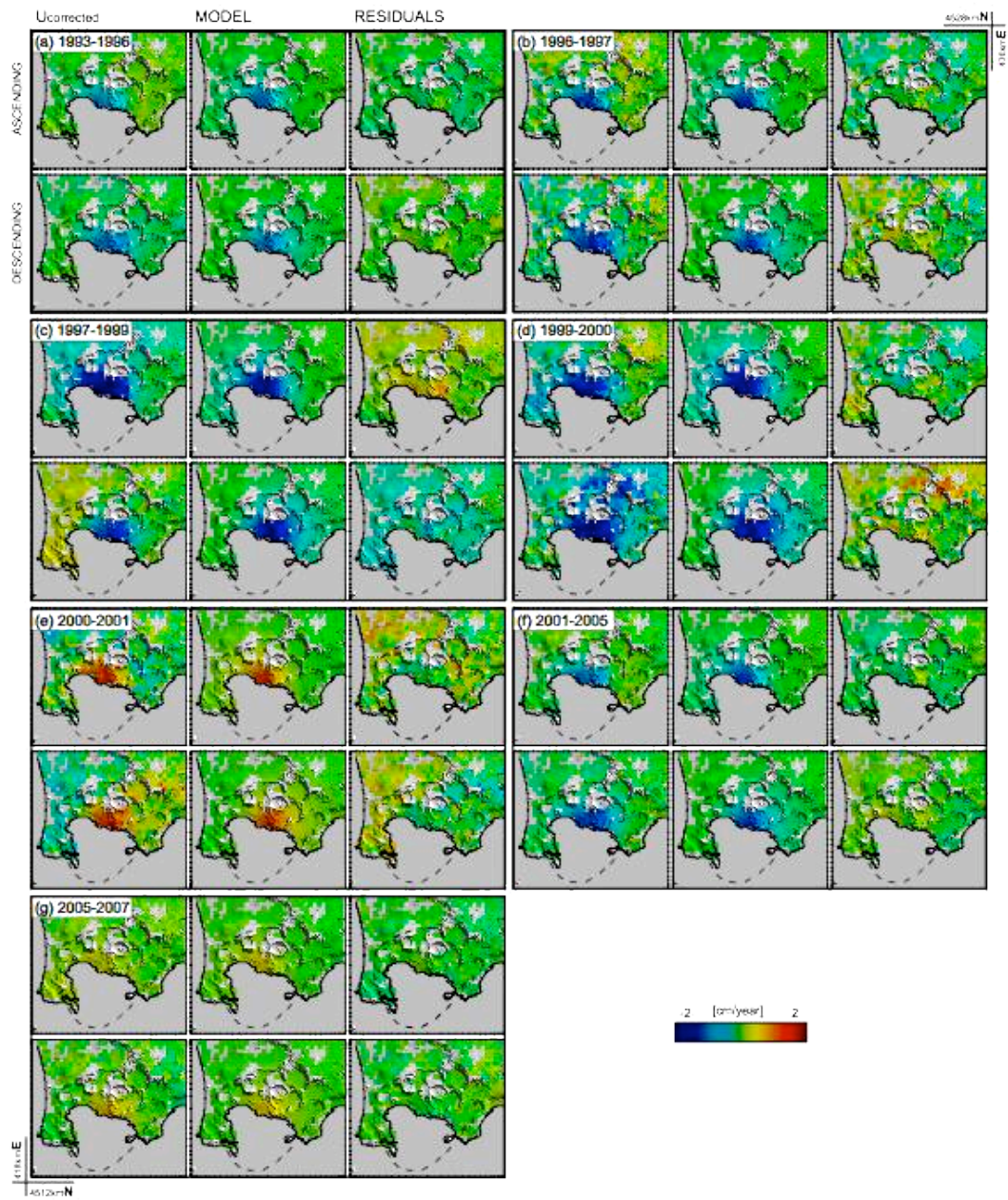


Figure 4.5: Results of the inversion after the application of the “correction” function to take into account the 3-D material heterogeneities. (a-g) Data corrected ($U_{corrected}$), models and residual maps representative of the entire analysis of the deformation at Campi Flegrei caldera in the period 1992-2008. See also text for more details.

Table 4.2

Period	East [km]		North [km]		Depth [km]		ΔV [Mm ³ /yr]		rms [cm]
	Min	Max	Min	Max	Min	Max	Min	Max	
93-96	426.3	426.6	4519.1	4519.6	2.5	3	-0.49	-0.46	0.12
96-97	426.3	426.5	4518.7	4519.4	2.7	3.2	-0.74	-0.65	0.26
97-99	426.6	427.3	4519.2	4520	2.6	3	-1.05	-0.88	0.33
99-00	426.4	426.8	4519.5	4520.2	3.4	3.5	-1.3	-1.25	0.27
00-01	426.3	427.2	4518.9	4519.1	2.5	3	0.53	0.7	0.31
01-05	426.2	426.7	4519	4519.4	2.6	3	-0.7	-0.63	0.16
05-07	425.9	426.5	4519	4519.2	2.8	3	0.31	0.32	0.12

Table 4.3

Period	East [km]		North [km]		Depth [km]		ΔV [Mm ³ /yr]		rms [cm]
	Min	Max	Min	Max	Min	Max	Min	Max	
93-96	426.5	426.6	4520	4520.2	2.5	3	-0.35	-0.28	0.12
96-97	426.2	426.9	4519.5	4520.7	2.5	3.1	-0.45	-0.37	0.26
97-99	426.8	427.3	4520.1	4520.8	2.6	2.9	-0.68	-0.59	0.31
99-00	426.6	427	4520	4520.9	2.9	3.4	-0.92	-0.83	0.30
00-01	426.5	427.2	4519	4520.2	2.5	3	0.3	0.48	0.31
01-05	426.2	426.7	4519.2	4519.7	2.6	3	-0.47	-0.39	0.14
05-07	426.1	426.7	4518.6	4520.5	3	3.2	0.21	0.29	0.12

Table 4.2: Source parameters resulting from the inversion of the Campi Flegrei deformation (U_{InSAR}) assuming the standard approach. Table 4.3: Source parameters resulting after the correction for the 3-D heterogeneities ($U_{corrected}$). See also figure 4.5 and 4.6.

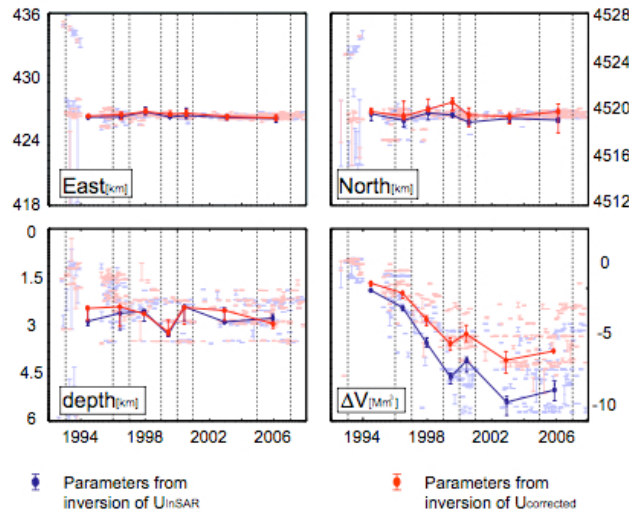


Figure 4.6: Parameters of the source of the deformation revealed at Campi Flegrei caldera in the period 1992-2008. In blue, the parameters of the best fitting models using the standard approach (U_{InSAR}). In red, the parameters of the best fitting models after the application of the “correction” function to take into account the 3-D mechanical heterogeneities of the area ($U_{corrected}$). In the background, shaded, results relative to the inversion of the cumulative displacements. In the foreground, results relative to the inversion of the data stacks, as best representative of the whole analysis (see text and also figure 4.5 a-g for details). Error bars represent the range of values that the parameters assumed within the 10% of the minimum cost. The assumption of homogeneity causes an over-estimation of the ΔV at depth up to 35%.

4.4. SUMMARY AND DISCUSSION

In this work, we constructed 3-D finite element models representative of the mechanical setup of the caldera (3DHET), considering a realistic vertical and lateral distribution of mechanical heterogeneities derived from seismic tomography. Simplified homogeneous half-space models (HHS), used in synthetic tests for the interpretation of surface deformation generated within 3DHET, achieved very good assessment of the source location but remarkable overestimation of the source volume change. Thus, we proposed a procedure to “correct” the measured data, allowing the use of homogeneous models to retrieve in a fast and reliable way source parameters as they were calculated in a fully 3-D heterogeneous medium. As an application, we analyzed the ground displacements measure at CF caldera in the period 1992-2008 with an SBAS-DInSAR analysis. The dilatation and contraction of a small spherical source, almost stable in position during the entire period of observation, is able to well explain the deformation signal over space and time, achieving small differences between the modeled and the observed data.

In the following, we discuss the limitations and the validity of our modeling assumptions, and compare our results to previous studies focusing on the implications on the reservoir size and shape, and on the evolution of pressures at depth associated with the surface deformation at CF caldera.

4.4.1. Mechanical setup: 3-D vs. 1-D layering

Our synthetic tests using FE models evidenced the importance to take into account 3-D mechanical heterogeneities for the interpretation of surface displacements at CF caldera. Recent studies analyzed the influence of 1-D layering on the estimation of source parameters at CF caldera (Crescentini et al., 2007). We compared our 3DHET model with an approximated 1-D layered configuration, finding that the latter attains displacements up to 15% smaller in the inner caldera. Hence, a more realistic mechanical setup detailed from the 3-D tomography study, as considered in our FE models, provides better constraints on the strain behavior of the CF caldera. The geometric structure

of the softer caldera basin, bounded by the stiffer periphery, locally amplifies the surface displacements and leads to major differences while compared with a uniform horizontal layered configuration. Such effects are to some extent analogous to those hypothesized by other authors as the consequence of ring fault dislocation, which, similarly to sharp mechanical contrasts, may cause amplifications and discontinuities on CF caldera stress and strain field (Beauducel et al., 2004).

4.4.2. Elastic properties: Dynamic vs. Static

The mechanical properties derived from seismic tomography might be biased by the resolution of the tomographic study itself. Nevertheless, we consider the velocity model of Chiarabba and Moretti (2006) to date one of the best available representations of the 3-D structure of CF caldera. An improvement of the resolution of tomographic analysis may allow constructing FE models with a more detailed mechanical setup, thus a better assessment of 3-D heterogeneities effects. However, the elastic constants derived from seismic velocities are representative for the undrained response of rocks to a dynamic stress solicitation. Deformation caused by volcanic sources, in turn, assumes a relatively constant application of stress over a longer time. Therefore, the consideration of static and drained response would be more appropriate in the analysis of the displacement field (Heap et al., 2008). Specific laboratory tests constraining static elastic properties for CF caldera are unfortunately at the moment not available. Static versus dynamic mechanical parameters might be in some cases very similar, but they might also differ by up to 1-2 order of magnitude, especially where the materials are subjected to plastic rather than pure elastic deformation (McCann and Entwisle, 1992; Soroush and Fahimifar, 2003). Thus, the elastic mechanical parameters herein used, in agreement with those derived using ultrasonic logs in laboratory experiments, might be considered as an upper limit for the material properties of CF caldera (Zamora et al., 1994).

The assumption of drained response of rocks to stress solicitations would imply the assumption of Poisson's ratio $\nu=0.25$ throughout the models (e.g. Trasatti et al., 2005). However, recent laboratory experiments on volcanic rock samples have shown that cyclic loading may increase ν by up a factor of

3, independently on drained or undrained conditions (Heap et al., 2008). For this reason, it is difficult to distinguish what might be the causes of the relatively large values of v resulting from the conversion of the seismic velocities, as in the upper levels of CF caldera. In fact, they might be related not only to the presence of fluids, hence undrained response, but also due to the effects of cyclic loading caused by the recurrent uplift and subsidence phases experienced by this area. We note, however, that the consideration of $v=0.25$ in the whole domain of 3DHET had no remarkable effects on our final results.

Time-and-temperature dependent material properties, as poroelastic, viscoelastic and viscoplastic behavior might also have major effects on CF caldera strain behavior, hence on the evaluation of source processes (Bonafede, 1991; De Natale et al., 1991). The parameters to accomplish more detailed analyses are still poorly constrained. Further investigations are needed to better assess the effects of such complexities on behavior of the source and of the deformation field at CF caldera.

4.4.3. “Correction” functions: a new method to take into account material complexities?

After the results of our numerical tests, we demonstrated that the application of the specific “correction” function to the real displacements measured at CF caldera prior to the inversion might be considered as a convenient way to take into account material heterogeneities effects. Similar approaches are used in seismology for several applications. For example, “station corrections” are applied to compensate the effects of lateral variations in the crust and uppermost mantle on wave travel times (Wright, 2008 and references therein). The 3-D heterogeneity effects may be taken into account also using the FE models directly within the optimization algorithm; however, such inverse problems are still computationally very expensive. The analysis of large datasets, as the 16-years time series for CF caldera here presented, would have been impossible due to tremendous computational times. The big advantage of this technique is that, after the determination of the “correction” function, fast and reliable assessment of source parameters might be still performed using HHS models. Moreover, the results of our ongoing tests

using the FE as source models in the optimization procedure are so far in agreement with these obtained using the “correction” function. Hence, the use of a “correction” procedure in combination with simplified analytical modeling would be a convenient way especially for monitoring purposes, where a fast and reliable quantitative analysis is needed. The same method is applicable not only to the SBAS-DInSAR dataset, but also to any other geodetic signal measured in the area. Moreover, while the position and the geometry of the source of the deformation at CF caldera appear to be yet well constrained, if in future no dramatic changes occur, the analysis might be done using more straight forward algorithms, because the parameter to be constrained would be only one, i.e. the volume change. Since CF caldera experienced also recently ground uplifts of several meters, these differences might play a relevant role for a quantitative and correct assessment of a hazard potential. In other volcanic areas, where similarly as CF mechanical heterogeneities might not affect the estimation of the source location and geometry, a similar approach could be considered. We hypothesize that for other calderas, which in general present an inner basin with softer mechanical properties derived from the infill sediments and bounded by stiffer materials on the rims (e.g. Yellowstone or Long Valley), an analogous behavior as here presented for CF might be expected. However, for a quantitative analysis, a priori geophysical investigations and numerical tests are necessary in order to characterize the “real” mechanical behavior for every volcanic area.

Furthermore, we note that the effects estimated from other authors as caused on volcano deformation by the topographic relief are very similar to those herein explained for the 3-D heterogeneities, i.e. affect mostly the ΔV estimations (cf. Cayol and Cornet, 1998; Meo et al., 2008). In this context, “correction” functions might be calculated also to attain topographic corrections. This would apply not only for the spherical source models, but also for ellipsoidal and dislocation planes, since the relationship between surface displacement and source strength in elastic models is linear.

4.4.4. Constraints on the evolution of pressures at depth in the last 16 years

One of the peculiarities of CF caldera is that subsidence phases are nearly a-seismic, while earthquake swarms usually accompany the uplift phases. This has been the case in the 1980s and also during the more recent unrests. The events are mostly localized in the center of the caldera, at depths between 2 and 4 km. The analysis of the seismicity recorded during the uplift phase of 2000-2001 indicates the reactivation of faults oriented NE-SW and NW-SE (Saccorotti et al., 2001; Bianco et al., 2004). The earthquakes have been related to an increase of hydrostatic fluid pressures within the CF caldera hydrothermal system, thought to be energetic enough to induce fluid migration and brittle failure of the rocks hosting the fluid-filled cavities. The expected pressure changes necessary to explain the observed reactivation of tectonic structures are in the order of about 10 to 30 MPa at 3 km depth (Bianco et al., 2004).

Combining this a priori information with the results of our analysis, we may derive more constraints for the geometry and dimensions of the reservoir responsible for the deformation observed at CF caldera in the past sixteen years. Indeed, the relationship between pressure change (ΔP) and volume change (ΔV) for a small spherical source is defined as:

$$\Delta P = \frac{\Delta V \mu}{a^3 \pi} \quad (4.2)$$

where a is the radius of the source and μ is the elastic shear modulus.

Using this relationship, we may convert the values of ΔV , constrained by the results of our optimization procedure, and retrieve the relative ΔP . Figure 4.7 shows the evolution of ΔP at CF caldera occurring at depths of about 3 km in the period between 1992 and 2008. The selection of a proper average μ representative of CF caldera is difficult, realistic values span the range between 1 GPa and 15 GPa (Trasatti et al., 2008 in press; Amoruso et al., 2008). We herein considered an average of the mechanical properties derived from the seismic tomography in the near field, i.e. ± 8 km from the center of the caldera up to 4 km depth, weighted by the resolution of the grid used for

the seismic tomography itself (1x1x1 km), i.e. $\mu=7$ GPa. In any case, to achieve pressure changes in agreement with the seismicity observed during the uplift periods, the source radius has to be smaller than 0.5 km. Such interpretation is valid only when considering a reservoir approximated as a small and spherical source (Mogi, 1958). We tested also different source models, finding that the position and ΔV of an ellipsoidal (Yang, 1988), rectangular- or penny-shaped reservoir (Okada, 1985; Fialko, 2001) is similar to the spherical one. This is in agreement with previous analysis of portions of the same SBAS dataset, analyzed using independent algorithms (Lundgren et al., 2001; Lanari et al., 2004; Trasatti et al., 2008). However, the estimation of the geometrical parameters associated to these more-complex source models is very uncertain and difficult to constrain. Nonetheless, tacking into account once more the a priori information available, in the center of the caldera at about 2.5-3.5 km depth a rather small source would be compatible with the V_p/V_s anomaly evidenced from seismic tomography and recent seismic reflection studies. Such anomaly has been interpreted as a rock volume filled with over-pressurized gas and fluids, probably related to the hydrothermal reservoir of the CF caldera system (Chiarabba and Moretti, 2006; Zollo et al., 2008). The former has been hypothesized to react in response to the activity of a deeper magmatic body (De Natale et al., 2006 and references therein). This interpretation is further supported by recently published geochemical data retrieved from the monitoring of the active fumarolic field over the same time period (Chiodini et al., 2009). We cannot exclude completely different source geometries or mechanism, such as the intrusion of magmatic bodies in the form of extended sill-shaped fractures (Amoruso et al., 2007). However, for a better discrimination between such processes other constraints have to be considered, e.g. variations of the gravity field associated with the deformation in the same time period of observation.

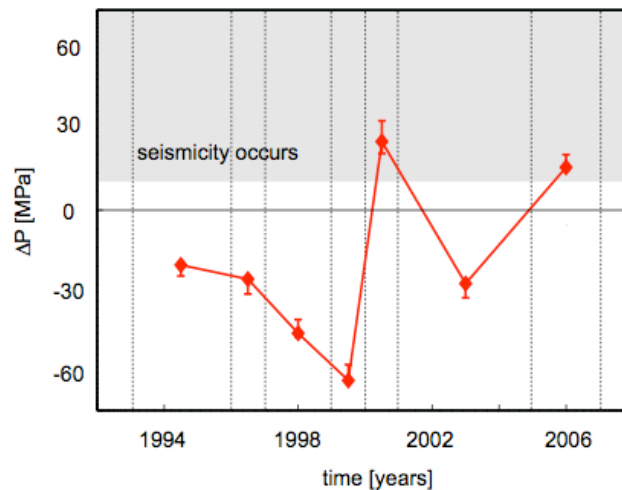


Figure 4.7: Evolution of source pressures at Campi Flegrei caldera between 1992 and 2008. According to Bianco et al., 2004, the seismicity at Campi Flegrei during 2000-2001 might be explained by a hydrostatic pressure change (ΔP) in the range of 10-30 MPa at 3 km depth. From the results of the inversion of the data stacks for representative periods over the past 16-years, corrected for the effects of 3-D heterogeneities (red diamonds), we achieve such ΔP range when considering $a=0.17$, 0.325 and 0.42 km for average $\mu=1$, 7 and 15 GPa, respectively. See also equation 4.2 and text for more details.

4.5. CONCLUSIONS

The main conclusions of this work might be summarized as follows:

1. In the study of surface deformations at CF caldera, the assumption of a homogeneous half-space does not affect the estimation of the source location, but might mislead the assessment of source's strength.
2. The surface deformation measured by means of geodetic techniques at CF caldera might be "corrected" with specific functions to take into account the effects of 3-D heterogeneities, and to obtain a fast and reliable way for accurate estimations of the source strength.
3. The analysis of the complete CF caldera SBAS-DInSAR dataset suggests that all the deformation observed between 1992 and 2008 is probably entirely related to the unrests of a small source located in the center of the caldera at about 3 km depth.
4. The pressure variations estimated in this study for the source of ground deformation at CF caldera are compatible with these believed to cause the

seismic swarms during the uplift periods, which are probably related to hydrostatic pressure variations occurred within the hydrothermal reservoir.

4.6. APPENDIX

The “correction” function for the displacements measured at CF caldera has been derived after several empirical tests performed using FE models. In this appendix, we explain the procedure adopted for such purpose. Starting from the analytical model of a small spherical cavity embedded in an elastic homogeneous medium (Mogi, 1958), we may write:

$$U_{(x,y,0)} = G \cdot s \quad (\text{A1})$$

where $U(x,y,0)$ are the surface displacements in a xyz coordinate system, G are the Green’s functions for displacements, which depend on the source position with respect to the free surface and on the half-space elastic properties, and s is the strength of the dilatation/contraction source. The latter might be described in terms of volume or pressure changes:

$$s = \Delta P(1 - \nu) \frac{a^3}{\mu} = \Delta V \frac{(1 - \nu)(1 + \nu)}{2\pi(1 - 2\nu)} \quad (\text{A2})$$

where ΔP and ΔV are the pressure and the volume change, respectively, a is the radius of the source, μ is the shear modulus and ν is the Poisson’s ratio which both depend on the elastic characteristics of the half-space (cf. Masterlark and Lu, 2004).

Setting up two FE models and considering for both same source parameters, i.e. location xyz and strength s , but different mechanical setups, using the same notation as for equation (A1) we may write:

$$U_{3DHET(x,y,0)} = G^*_{3DHET} \cdot S_{3DHET} \quad (A3)$$

$$U_{HHS(x,y,0)} = G^*_{HHS} \cdot S_{HHS}$$

where 3DHET and HHS stay respectively for the 3-D heterogeneous and for the average homogeneous half-space mechanical configurations, and G^* stays for the reduced Green's functions, which now depend only on the elastic constants. Due to the linear relationship between the surface displacements and the source strength when linear elastic material is assumed, we may write:

$$K_{(x,y,0)} = \frac{U_{3DHET(x,y,0)}}{\max(U_{HHS(x,y,0)})} - \frac{U_{HHS(x,y,0)}}{\max(U_{HHS(x,y,0)})} \quad (A4)$$

Formula (A4) is representative of the normalized difference between the two assumed mechanical setups, while:

$$w = \frac{\max(U_{3DHET(x,y,0)})}{\max(U_{HHS(x,y,0)})} \quad (A5)$$

is a weighting factor representative of amplification (positive) or decrease (negative) of the surface displacements. In a real case, we measure the surface deformations with a geodetic technique, e.g. DInSAR (U_{InSAR}). Assuming that the 3DHET model achieves a realistic representation of the deformations occurring in reality, we may substitute U_{3DHET} with U_{InSAR} , and thus derive:

$$U_{corrected(x,y,0)} = U_{InSAR(x,y,0)} - \frac{K_{(x,y,0)} \cdot \max(U_{InSAR(x,y,0)})}{w} \quad (A6)$$

The values of K calculated for the three components of the displacement field, and also projected on ascending and descending viewing geometries at the SBAS stations, are shown on figure A1. The factor w assumes the value 1.32 for the ascending and 1.34 for the descending viewing geometries. K and w depend strictly on the dimension of the source, hence in our case on the radius, and on the average value of the shear modulus μ selected as HHS representative for the 3-D heterogeneous distribution. We tested several radii in the range of values compatible for CF caldera (see section 4.4), finding that at parity of ΔV differences on surface deformations are smaller than 0.1 mm. In summary, if the material properties are not affecting the estimation the source location, and if the position of the source is not changing during the period of observation, as demonstrated from the analysis of the SBAS-DInSAR dataset of CF caldera, the inversion of $U_{\text{corrected}}$ retrieves values of ΔV corrected for the effects of 3-D mechanical heterogeneities.

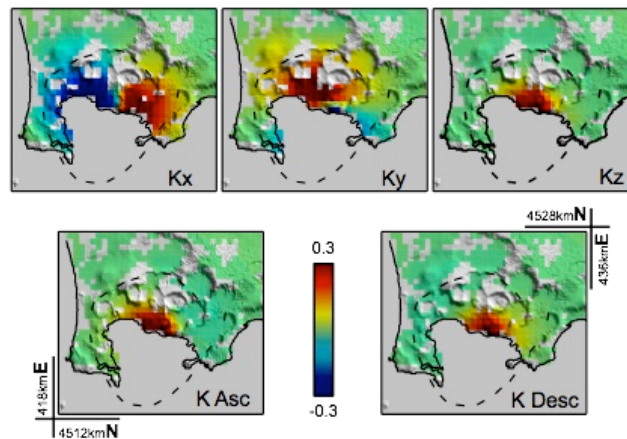


Figure A1: Correction functions superimposed on the Digital Elevation Model of the Campi Flegrei caldera for the three components of the displacement field (K_x , K_y , and K_z) and projected on the ascending (K_a) and descending (K_d) satellite viewing geometries.

Final remarks and future research developments

The motivation of this work is deep-rooted on a background of several recent publications about the effects of material complexities on stress and strain field at volcanoes, remarking a particular attention of the scientific community on this topic. In volcano geodesy, the advent of monitoring using GPS and InSAR widened our capability to observe over space and time features that before were impossible to detect. This completely changed the perspective: from a static, 1-D and mostly field-based approach, to the possibility to observe the dynamics of an ongoing volcanic process in 4-D and nearly real time from space-based techniques. In this context, there is a real need to develop new tools to better analyze and understand such complexities.

For this reason, the finite element method (FEM) is starting to be more and more used, especially because of its flexibility and for the possibility to implement a comprehensive Multiphysics environment. This is corroborated by the development of computer science, which improved substantially the standard available computational capacity. However, one of the big limitations for the application of the FEM to the Earth science is the poor knowledge of the properties of the subsurface, and especially in active volcanic areas, where the investigations are further limited by difficult access and hostile environmental conditions. Moreover, the little information available contains several uncertainties, especially because of the coarse resolution yet achievable by geophysical studies.

In almost every field of engineering, the results and interpretations of finite element models are used for prediction only after a systematic experimental validation. For example, crash-tests in automotive or aeronautical engineering are performed in reality in order to crosscheck the results of computer simulations and vice versa. In volcano geodesy, if the main goal of the modeling attempts is the process understanding in order to predict an event, to prevent a hazard or to evaluate a risk, the same philosophy should be considered. However, the improbable opportunity to verify empirically the

goodness of the models makes challenging the derivation of realistic and definitive interpretations. Despite the difficulties, finite element models may provide several hints, especially when testing the reliability of standard tools currently used for evaluation, such as the studies herein presented and discussed. In the next years the research in volcano geodesy will be probably oriented on the developing of physical models that take into account complex dynamics, in order to fill the enormous gap with the accuracies achieved by the observational and monitoring techniques. This can be achieved only with a multidisciplinary approach, which includes the experiences and the strengths of disciplines spanning from the theoretical physics to the applied engineering. In this context, we do not have to forget the field-based studies, which will play always a key role, being indispensable to accomplish a comprehensive evaluation of volcanic phenomena.

GSA Data repository: supplementary information for chapter 2

The following supplementary material includes:

1. Details of magma density calculations procedures.
2. Details on construction of the finite element models and the assumed loading/unloading conditions.
3. Details on the effects of different magma reservoir shapes.
4. Details on limitations and the validity of the finite element models.
5. Discussion of the possible effects of mass-wasting on melt production beneath ocean island volcanoes.
6. Supplementary References.
7. Supplementary Tables and Figures:

Table DR1: sampling/outcrop localities, respective rock type and, where available, calculated density. Table DR2: Geometrical parameters used for the finite element simulations of the conical edifice and that of volcano flank collapse. Figure DR1: Effect of melt%. Figure DR2: Effect of shape of magma storage zone on decompression.

1. Magma density calculations procedures

Volcanic products of El Hierro were collected during two field campaigns and were subsequently analyzed for whole-rock and groundmass major element compositions. We estimated pre-eruptive magma densities for representative El Hierro samples (see Table DR1), following the procedure outlined by Spera (2000) and using initial volatile contents approximated on the basis on Dixon et al. (1997). That is, dissolved water contents were taken as $H_2O=3(P_2O_5)$ wt% and initial carbon dioxide as $CO_2=2(H_2O)$ by mass. El Hierro samples give a range of $H_2O=1.4-4.0$ wt% and $CO_2=2.8-7.9$ wt%, comparable to bulk volatile contents inferred by Dixon et al. (1997), for undegassed alkaline Hawaiian magmas. For the density calculations, we assumed $fO_2=QFM+1$,

P=900 MPa (typical pressure of the main magma storage zone under Canarian shield volcanoes, see e.g. Klügel et al. 2005, Longpré et al. 2008 and Stroncik et al. 2008), and melts at their liquidus temperature, calculated using PETROLOG (Danyushevsky, 2001). The presence of phenocrysts in magma was also taken into account. For samples with <10 vol. % olivine + clinopyroxene, the density of the melt was taken as a reasonable approximation of the magma density. For samples with >10 vol. % olivine + clinopyroxene, the magma density was calculated using a melt density of 2,780 kg/m³ (average from groundmass samples) and observed modal phenocryst proportions (p_{olivine}=3,400 kg/m³ (~Fo80) and p_{clinopyroxene}=3,200 kg/m³). Plagioclase (due to its density nearly equal to melt density) as well as Fe-Ti oxide and amphibole (due to their small abundances) were considered negligible for these calculations.

2. Construction of the finite element models, loading/unloading conditions and mechanical properties

The finite element models described and discussed in our study were constructed using the commercial software ABAQUS™. The software and the relative “Analysis User's Manual” are available at www.simulia.com. For simplicity, the models are axisymmetric (as shown in Fig. 2a), thus the edifice load was applied as a triangular load using the formulation:

$$L(r) = \rho_v \cdot g \cdot H_i \cdot \left(1 - \frac{r}{R}\right) \quad (\text{DR1})$$

where L(r) is the load calculated at the radial coordinate (r), ρ_v is the density of the volcanic material (2,700 kg/m³), g is the gravitational acceleration (9.81 m/s²), H_i is the initial height of the edifice (6 km) and R is the radius at the base of the edifice (30 km, cf. Gee et al., 2001). In a second step, we removed 3% of the initial load equivalent to 180 km³ (see also Table DR2). Both the loading and the unloading step were simulated using the FORTRAN user subroutine *DLOAD. Far field boundary conditions were applied by means of a set of infinite elements on the right side and at the bottom of the models. The maximum dimension of the elements in the areas of interest for

pressure calculations was set to 100 m, as the best compromise between resolution and computational time (Fagan, 1992).

Geometrical parameters H_i and R used to calculate the initial loads for all localities were either collected from literature information or approximated based on analysis of digital elevation models or bathymetric maps (see Table DR2). This procedure may have introduced uncertainties in initial edifice volume estimates. On the other hand, flank collapse volumes considered in this study are well constrained. And in our simulations, effects due to collapse are distributed over the entire edifice, while in reality, they are likely to concentrate on particular portions of the volcanic system. For example, the effects of the El Golfo debris avalanche were probably much more focused on the El Golfo volcano (~2,000 km³) than on the whole El Hierro edifice (~5,500 km³), which would have led to a higher effective unloading fraction on the former. For this reason, the assumption of the unloading volume as portion of the total edifice compensate for the potential error on the estimation of the initial volume. The effects of the seawater load and of material redistribution due to collapse were also tested and found to only slightly decrease the retrieved pressure changes (cf. Pinel and Jaupart, 2005).

The mechanical behavior of a magmatic reservoir is commonly simulated treating magma as an incompressible fluid, with bulk modulus varying between 1 and 10 GPa (Blake, 1981; Huppert and Woods, 2002; Pinel and Jaupart, 2005). In our models, however, we consider El Hierro's magma storage zone as a multiphase system, with its effective elastic response being dependent on the percentage of melt present within it (Ryan, 1980). This assumption is in agreement with the magma plumbing system thought to exist beneath El Hierro (Stroncik et al., 2008), where, as proposed for other Canary Island volcanoes (Klügel et al., 2005; Longpré et al., 2008) and for Kilauea volcano, Hawaii (Tilling and Dvorack, 1993), magma may be stored in a plexus of dyke- and sill-like fractures in the uppermost mantle.

The assumption of a layered lithosphere might affect the pressure changes at shallow levels but, in our tests, has no major effect on the magma reservoir surroundings. Based on these considerations, we can state that our results give a conservative but realistic representation of static pressure changes caused by surface mass-wasting at the discussed volcanoes.

3. Effects of melt % and of different shape of magma reservoir

Figure DR1 and DR2 show the pressure changes in a profile beneath the edifice, corresponding to the axis of symmetry of the finite element models.

In DR1 we compare the decompression caused by the El Golfo landslide while occurring in a homogeneous half-space or in models that consider the presence of basaltic magmas at about 20 km depth. An increase of the melt percentage in the storage zone (DR1b) causes a decrease of the elastic stiffness, but an increase of the incompressibility. Such a behavior has been simulated in our models decreasing the effective Young's modulus and increasing the effective Poisson's ratio of the material, as described in Ryan, (1980). Higher percentage of melts may enhance the effects of the unloading due to mass-wasting.

In DR2 we compare the decompression occurring in a homogeneous half-space with models that consider a range of shapes for the simulated magma storage zone. Here, material properties inside the reservoir reflect an average basaltic magma with an overall melt percentage of 40%. Oblate-shaped (OS) reservoirs tend to favor slightly higher pressure changes compared with spherical-shaped (SS) or prolate-shaped (PS) reservoirs. However, the general directions of the vectors (i.e. from the bottom to the top of the reservoir) as well as the magnitudes of the differential pressure are largely unaffected.

4. Limitations and validity of the models

High pressures and temperatures, co-existence of several polyphase aggregates, volatiles and fluids add complexity to the analysis of magma reservoir feedback processes using simplified mechanical models. Nevertheless, for short time-scales, we consider the assumption of an elastic regime appropriate, as that of the magma reservoirs as zones of structural weakening causing localization of stresses (Kanamori, 1972; Gudmundsson, 1988). On longer time-scales, viscoelastic response may also play an important role in determining the amount of stress changes in the magma reservoir surroundings (Newman et al., 2006). Moreover, improved geometries of the edifices, collapse scars and magma plumbing systems would allow more refined quantitative evaluations of pressure changes due to

volcano flank collapse. More complex dynamic modeling and material properties, on the other hand, would allow better assessment of feedback processes caused by the pressure gradients revealed by our simulations. However, we argue that none of these potential improvements would change the principal outcome of our work.

5. Possible effects on melt production at ocean island volcanoes

Jull and McKenzie (1996) have shown that ice unloading during deglaciation can cause increased melt production in Iceland's spreading ridge system (see also Maclennan et al., 2002). Using numerical models, these authors found that, despite largest decompression amplitudes just below the ice sheet ($\Delta P = 20$ MPa), the maximum effect on mantle melting was actually much deeper, at a depth of about 80 km. In the presence of both a mantle plume and a spreading ridge, the young Icelandic crust and lithosphere are warmer and more ductile than old oceanic or continental upper mantle. The resulting melting interval is thus thick (about 100 km), from the base of the crust at 20 km depth to the solidus at about 115 km depth. The Icelandic case therefore differs considerably from pure hot-spot settings without spreading ridge, such as Hawaii or the Canary Islands. There, the older and colder oceanic lithosphere results in a significant mechanical boundary layer. Under these conditions, the melting zone is thinner and restrained at much greater depth, i.e. in the spinel and garnet (mostly) stability fields between about ~70-140 km depth (Watson and McKenzie, 1991; Hoernle and Schmincke, 1993).

The above-mentioned considerations, combined with the results of our numerical models, which imply negligible decompression at depths of magma generation, suggest that the unloading due to large-scale volcano flank collapse is unlikely to cause effects of similar magnitude on ocean islands as has been described for deglaciation periods on Iceland.

Supplementary Tables and Figures:

	Latitude (°N)	Longitude (°W)	Altitude (m)	Stratigraphy	Lava Type	Calculated Magma Density (kg/m ³)
1	27,73019	18,05931	1382	post-EGL	Basalt	–
2	27,73083	18,05921	1381	post-EGL	ankaramite	–
3	27,73133	18,05939	1372	post-EGL	ankaramite	–
4	27,72932	18,05962	1371	post-EGL	Basalt	–
5	27,73137	18,05931	1370	post-EGL	ankaramite	–
6	27,73288	18,06004	1368	post-EGL	ankaramite	–
7	27,73246	18,05962	1368	post-EGL	ankaramite	–
8	27,73319	18,06025	1366	post-EGL	ankaramite	–
9	27,73270	18,05985	1365	post-EGL	ankaramite	2970
10	27,73338	18,06026	1361	post-EGL	ankaramite	–
11	27,73227	18,05908	1355	post-EGL	ankaramite	–
12	27,73158	18,05857	1355	post-EGL	ankaramite	–
13	27,73028	18,05850	1347	post-EGL	basalt	2870
14	27,72953	18,05870	1338	post-EGL	basalt	2730
15	27,73271	18,05805	1335	post-EGL	ankaramite	–
16	27,72820	18,05807	1327	post-EGL	basalt	2740
17	27,73317	18,05791	1326	post-EGL	ankaramite	–
18	27,72806	18,05817	1325	post-EGL	basalt	–
19	27,73385	18,05820	1310	post-EGL	ankaramite	–
20	27,72886	18,05250	1262	post-EGL	basalt	2680
21	27,73010	18,05216	1261	post-EGL	basalt	–
22	27,73165	18,05142	1243	post-EGL	basalt	–
23	27,77451	17,94374	1003	post-EGL	basalt	–
24	27,74072	18,05241	934	post-EGL	basalt	–
25	27,73977	18,04936	934	post-EGL	basalt	–
26	27,73937	18,04603	933	post-EGL	basalt	–
27	27,74119	18,05684	895	post-EGL	ankaramite	–
28	27,74164	18,06080	878	post-EGL	ankaramite	–
29	27,74064	18,06523	849	post-EGL	ankaramite	–
30	27,73991	18,03150	847	post-EGL	basalt	–
31	27,73992	18,03151	847	post-EGL	ankaramite	–
32	27,73977	18,02964	832	post-EGL	ankaramite	–
33	27,74014	18,06725	831	post-EGL	ankaramite	–
34	27,73954	18,06931	825	post-EGL	ankaramite	–
35	27,73852	18,07070	810	post-EGL	basalt	–
36	27,73778	18,07189	806	post-EGL	ankaramite	–
37	27,73699	18,07699	801	post-EGL	ankaramite	–
38	27,73689	18,07260	796	post-EGL	ankaramite	–
39	27,73600	18,07367	791	post-EGL	ankaramite	–
40	27,73867	18,02507	785	post-EGL	ankaramite	–
41	27,75332	17,98959	762	post-EGL	basalt	–
42	27,75334	17,98994	745	post-EGL	basalt	–
43	27,75341	17,99020	718	post-EGL	basalt	–
44	27,75354	17,99068	686	post-EGL	basalt	–

45	27,75346	17,99136	650	post-EGL	basalt	-
46	27,75168	17,99258	633	post-EGL	basalt	-
47	27,75229	17,99379	557	post-EGL	basalt	-
48	27,74473	18,02584	540	post-EGL	ankaramite	-
49	27,74486	18,10117	450	post-EGL	basalt	-
50	27,74500	18,10090	430	post-EGL	basalt	-
51	27,75355	18,00350	379	post-EGL	basalt	-
52	27,75127	18,05506	276	post-EGL	ankaramite	2940
53	27,74722	18,08758	264	post-EGL	ankaramite	-
54	27,74695	18,08646	261	post-EGL	ankaramite	-
55	27,74810	18,09251	257	post-EGL	ankaramite	-
56	27,74708	18,08386	257	post-EGL	ankaramite	-
57	27,74709	18,08387	257	post-EGL	plag. basalt	-
58	27,75028	18,06707	256	post-EGL	ankaramite	-
59	27,74660	18,07963	242	post-EGL	ankaramite	2890
60	27,75024	18,06703	241	post-EGL	ankaramite	-
61	27,75052	18,01094	190	post-EGL	aphyric basalt	2620
62	27,75223	18,09663	134	post-EGL	basalt	-
63	27,78235	18,00092	44	post-EGL	ankaramite	2910
64	27,75696	18,10941	13	post-EGL	basalt	-
65	27,72587	18,02609	1342	uncertain	aphyric basalt	-
66	27,72339	18,03004	1315	uncertain	aphyric basalt	-
67	27,72202	18,02584	1269	uncertain	basalt	-
68	27,72195	18,02414	1264	uncertain	aphyric basalt	-
69	27,71388	18,01479	1257	uncertain	basalt	-
70	27,72250	18,02218	1252	uncertain	basalt	-
71	27,72443	18,08560	1189	uncertain	ankaramite	-
72	27,72297	18,08508	1147	uncertain	ankaramite	-
73	27,72298	18,08509	1147	uncertain	aphyric basalt	-
74	27,71270	18,01911	1121	uncertain	basalt	-
75	27,72532	18,09079	1106	uncertain	aphyric basalt	2640
76	27,71311	18,02191	1090	uncertain	basalt	-
77	27,71009	18,02308	1042	uncertain	aphyric basalt	-
78	27,72260	18,09134	1025	uncertain	aphyric basalt	-
79	27,72261	18,09135	1025	uncertain	ankaramite	2940
80	27,72084	18,08935	1006	uncertain	ankaramite	-
81	27,71295	18,02842	1002	uncertain	basalt	-
82	27,71330	18,03263	970	uncertain	basalt	-
83	27,71888	18,09406	936	uncertain	ankaramite	-
84	27,71889	18,09407	936	uncertain	aphyric basalt	-
85	27,71264	18,03741	932	uncertain	aphyric basalt	-
86	27,71323	18,03857	928	uncertain	basalt	-
87	27,72066	18,09779	906	uncertain	ankaramite	-
88	27,72067	18,09780	906	uncertain	basalt	-
89	27,72369	18,10361	852	uncertain	basalt	-
90	27,72370	18,10362	852	uncertain	ankaramite	-
91	27,79772	17,96879	829	uncertain	basalt	-
92	27,79773	17,96880	829	uncertain	ankaramite	-
93	27,72468	18,10689	826	uncertain	ankaramite	-
94	27,73771	17,95242	809	uncertain	aphyric basalt	-

95	27,69630	18,00453	799	uncertain	aphyric basalt	–
96	27,73738	17,95302	798	uncertain	basalt	–
97	27,69747	17,99642	785	uncertain	ankaramite	–
98	27,69651	17,99954	785	uncertain	ankaramite	–
99	27,69670	18,01235	782	uncertain	basalt	–
100	27,73633	17,95210	728	uncertain	basalt	–
101	27,70085	18,02648	712	uncertain	basalt	–
102	27,73576	17,95233	704	uncertain	basalt	–
103	27,72735	18,11848	693	uncertain	aphyric basalt	–
104	27,68669	17,98540	674	uncertain	aphyric basalt	–
105	27,73526	17,95251	643	uncertain	basalt	–
106	27,68589	17,98722	642	uncertain	ankaramite	–
107	27,68488	17,98928	627	uncertain	basalt	–
108	27,68334	17,99472	576	uncertain	ankaramite	–
109	27,68145	17,99572	551	uncertain	basalt	–
110	27,73410	17,95331	545	uncertain	basalt	–
111	27,81238	17,96622	524	uncertain	ankaramite	–
112	27,68382	18,00867	517	uncertain	basalt	–
113	27,68240	18,00198	514	uncertain	basalt	–
114	27,68235	18,00557	509	uncertain	basalt	–
115	27,73347	17,95434	497	uncertain	basalt	–
116	27,68439	18,01318	490	uncertain	aphyric basalt	–
117	27,78937	17,92105	479	uncertain	aphyric basalt	–
118	27,68597	18,01764	470	uncertain	basalt	–
119	27,68598	18,01765	470	uncertain	ankaramite	–
120	27,73282	17,95438	449	uncertain	basalt	–
121	27,73791	18,14196	379	uncertain	ankaramite	–
122	27,73163	17,95443	361	uncertain	basalt	–
123	27,74719	18,14456	334	uncertain	ankaramite	–
124	27,72349	18,14470	310	uncertain	aphyric basalt	–
125	27,74796	18,14239	307	uncertain	ankaramite	–
126	27,74797	18,14240	307	uncertain	basalt	–
127	27,73107	17,95418	302	uncertain	basalt	–
128	27,75426	18,14399	248	uncertain	ankaramite	2960
129	27,75427	18,14400	248	uncertain	aphyric basalt	2590
130	27,72990	17,95430	210	uncertain	aphyric basalt	–
131	27,72821	17,95438	174	uncertain	aphyric basalt	–
132	27,70738	18,14677	125	uncertain	basalt	2830
133	27,64695	17,99310	115	uncertain	basalt	2850
134	27,75660	18,14840	60	uncertain	ankaramite	3020
135	27,75839	18,14964	33	uncertain	ankaramite	–
136	27,72521	18,05244	1464	pre-EGL	basalt	–
137	27,72566	18,06711	1417	pre-EGL	ankaramite	2890
138	27,72740	18,04769	1407	pre-EGL	basalt	–
139	27,72550	18,04939	1407	pre-EGL	basalt	2870
140	27,72490	18,05349	1392	pre-EGL	plag. basalt	2600
141	27,72490	18,05349	1392	pre-EGL	ankaramite	2880
142	27,72649	18,05597	1346	pre-EGL	plag. basalt	–
143	27,72284	18,05528	1313	pre-EGL	ankaramite	–
144	27,72268	18,06655	1300	pre-EGL	ankaramite	–

145	27,72399	18,07506	1270	pre-EGL	ankaramite	2960
146	27,75856	17,97703	1248	pre-EGL	aphyric basalt	2550
147	27,75862	17,97679	1244	pre-EGL	ankaramite	3000
148	27,75862	17,97579	1233	pre-EGL	ankaramite	–
149	27,76259	17,98095	1201	pre-EGL	basalt	–
150	27,76165	17,98055	1167	pre-EGL	aphyric basalt	–
151	27,76132	17,98047	1155	pre-EGL	aphyric basalt	–
152	27,76138	17,98087	1125	pre-EGL	aphyric basalt	–
153	27,76063	17,98067	1109	pre-EGL	aphyric basalt	–
154	27,76019	17,98142	1089	pre-EGL	ankaramite	–
155	27,75930	17,98197	1070	pre-EGL	basalt	–
156	27,75878	17,98230	1065	pre-EGL	plag. basalt	–
157	27,75767	17,98235	1046	pre-EGL	plag. basalt	–
158	27,75843	17,98221	1045	pre-EGL	aphyric basalt	–
159	27,75697	17,98399	1001	pre-EGL	basalt	–
160	27,77583	17,94294	980	pre-EGL	aphyric basalt	2710
161	27,75615	17,98582	966	pre-EGL	ankaramite	–
162	27,77485	17,94344	957	pre-EGL	plag. basalt	–
163	27,77486	17,94345	957	pre-EGL	ankaramite	–
164	27,75604	17,98612	956	pre-EGL	basalt	–
165	27,75573	17,98677	935	pre-EGL	basalt	–
166	27,75554	17,98681	922	pre-EGL	basalt	–
167	27,75554	17,98693	903	pre-EGL	aphyric basalt	–
168	27,74435	18,11209	877	pre-EGL	basalt	–
169	27,75517	17,98689	869	pre-EGL	basalt	–
170	27,74401	18,11038	861	pre-EGL	aphyric basalt	–
171	27,75428	17,98788	853	pre-EGL	basalt	–
172	27,74349	18,10904	841	pre-EGL	basalt	–
173	27,74313	18,10879	825	pre-EGL	aphyric basalt	–
174	27,74275	18,10799	817	pre-EGL	basalt	–
175	27,75403	17,98850	808	pre-EGL	basalt	–
176	27,74276	18,10749	800	pre-EGL	basalt	–
177	27,74277	18,10750	800	pre-EGL	ankaramite	–
178	27,73707	17,95264	780	pre-EGL	ankaramite	–
179	27,74271	18,10605	773	pre-EGL	ankaramite	–
180	27,74239	18,10580	757	pre-EGL	ankaramite	–
181	27,79997	17,97989	755	pre-EGL	ankaramite	3010
182	27,74235	18,10518	743	pre-EGL	ankaramite	–
183	27,80082	17,98013	724	pre-EGL	basalt	2870
184	27,80067	17,98018	723	pre-EGL	ankaramite	–
185	27,80030	17,98034	706	pre-EGL	basalt	–
186	27,79943	17,98073	682	pre-EGL	basalt	–
187	27,74247	18,10239	668	pre-EGL	basalt	–
188	27,80663	17,97708	665	pre-EGL	ankaramite	–
189	27,79930	17,98102	648	pre-EGL	basalt	–
190	27,79931	17,98103	648	pre-EGL	ankaramite	–
191	27,74258	18,10237	645	pre-EGL	ankaramite	–
192	27,75256	17,99162	644	pre-EGL	basalt	–
193	27,75304	17,99124	643	pre-EGL	basalt	–
194	27,79895	17,98110	633	pre-EGL	basalt	–

195	27,74284	18,10129	624	pre-EGL	aphyric basalt	–
196	27,75268	18,11980	620	pre-EGL	ankaramite	–
197	27,75269	18,11981	620	pre-EGL	basalt	–
198	27,79840	17,98123	619	pre-EGL	trachyte	2420
199	27,79814	17,98132	607	pre-EGL	aphyric basalt	–
200	27,79803	17,98153	590	pre-EGL	plag. basalt	–
201	27,74324	18,10132	583	pre-EGL	ankaramite	–
202	27,79769	17,98152	569	pre-EGL	aphyric basalt	–
203	27,74351	18,10128	553	pre-EGL	aphyric basalt	–
204	27,79805	17,98188	545	pre-EGL	basalt	–
205	27,79836	17,98198	526	pre-EGL	plag. basalt	–
206	27,79784	17,98216	514	pre-EGL	trachyte	2360
207	27,74410	18,10112	506	pre-EGL	aphyric basalt	–
208	27,74411	18,10113	506	pre-EGL	ankaramite	–
209	27,79720	17,97977	500	pre-EGL	aphyric basalt	2710
210	27,79819	17,98223	499	pre-EGL	trachyte	–
211	27,79811	17,98249	497	pre-EGL	plag. basalt	–
212	27,74439	18,10109	489	pre-EGL	ankaramite	–
213	27,79774	17,98244	479	pre-EGL	aphyric basalt	–
214	27,79754	17,98206	471	pre-EGL	aphyric basalt	–
215	27,79728	17,98187	462	pre-EGL	basalt	–
216	27,74485	18,10116	450	pre-EGL	ankaramite	–
217	27,78659	17,92121	448	pre-EGL	ankaramite	2990
218	27,79697	17,98217	443	pre-EGL	basalt	–
219	27,79492	17,98298	434	pre-EGL	aphyric basalt	–
220	27,79567	17,98277	433	pre-EGL	basalt	–
221	27,74499	18,10089	430	pre-EGL	ankaramite	–
222	27,79469	17,98311	429	pre-EGL	aphyric basalt	–
223	27,79436	17,98340	419	pre-EGL	ankaramite	–
224	27,79437	17,98341	419	pre-EGL	basalt	–
225	27,79379	17,98363	404	pre-EGL	basalt	–
226	27,79322	17,98389	395	pre-EGL	basalt	–
227	27,79236	17,98451	379	pre-EGL	basalt	–
228	27,79186	17,98471	369	pre-EGL	basalt	–
229	27,79141	17,98510	360	pre-EGL	basalt	–
230	27,79142	17,98532	354	pre-EGL	aphyric basalt	–
231	27,79138	17,98556	336	pre-EGL	aphyric basalt	–
232	27,79140	17,98573	326	pre-EGL	aphyric basalt	–
233	27,79116	17,98613	307	pre-EGL	basalt	–
234	27,79060	17,98666	295	pre-EGL	basalt	–
235	27,78988	17,98464	290	pre-EGL	aphyric basalt	2720
236	27,79080	17,98679	279	pre-EGL	ankaramite	–
237	27,79081	17,98680	279	pre-EGL	basalt	–
238	27,79071	17,98704	249	pre-EGL	basalt	–
239	27,79025	17,98746	231	pre-EGL	basalt	–
240	27,78985	17,98797	219	pre-EGL	aphyric basalt	–
241	27,78944	17,98846	211	pre-EGL	basalt	–
242	27,78928	17,98900	179	pre-EGL	ankaramite	–
243	27,76695	17,91809	160	pre-EGL	aphyric basalt	2700
244	27,78864	17,98902	158	pre-EGL	basalt	–

Table DR.1: Outcrop localities investigated on El Hierro Island. Lava types are divided into four categories, according to modal mineralogy: 1) aphyric to sub-aphyric (<5 vol. % phenocrysts of olivine/clinopyroxene/plagioclase, called aphyric basalt); 2) plagioclase-phyric (5-40 vol. %, called plagioclase basalt, which is sometimes referred to as “trachytes” in the literature); 3) moderately olivine- and/or clinopyroxene-phyric (5-20 vol. %, called basalt) and 4) highly olivine-clinopyroxene-phyric (>20 vol. %, called ankaramites). In Figure 1, the first three types are encompassed under the “crystal-poor” category. Where available, stratigraphic position and calculated magma density is also given.

	Height [km]	Radius [km]	Edifice Volume [km ³]	Collapse Volume [km ³]	% of initial load
Augustine	~1.2 ^a	3.2 ^(*)	13 ^a	0.3 ^a	0.4%
St. Helens	1 ^(*)	6 ^(*)	38 ^b	2.5 ^c	6.5%
Parinacota	1.5 ^(*)	5.5 ^(*)	45 ^d	6 ^d	13%
Teno	5.3 ^e	25 ^e	3,500 ^(*)	~50 ^f	1,4%
El Golfo	6 ^g	30 ^g	5,500 ^h	~180 ^f	3%
Tahiti-Nui	4 ⁱ	50 ⁱ	10,500 ^(*)	~1,150 ^j	7%
Waianae	~6 ^(*)	63 ^(*)	25,000 ^k	~6,100 ^l	38%

Table DR.2: Geometrical parameters used for the finite element simulations of conical edifices that experienced a volcano flank collapse. (a) Siebert et al. (1995); (b) Voight et al. (1981); (c) McGuire (1996); (d) Hora et al. (2007) ; (e) Walter (2003) ; (f) Masson et al. (2002) ; (g) Gee et al. (2001); (h) Schmincke (1998) ; (i) Patriat et al. (2002) ; (j) Hildenbrand et al. (2004) ; (k) Robinson and Eakins (2006) ; (l) Presley et al. (1997).

() Other values have been either calculated from other known parameters or estimated from Digital Elevation Models and bathymetric maps.*

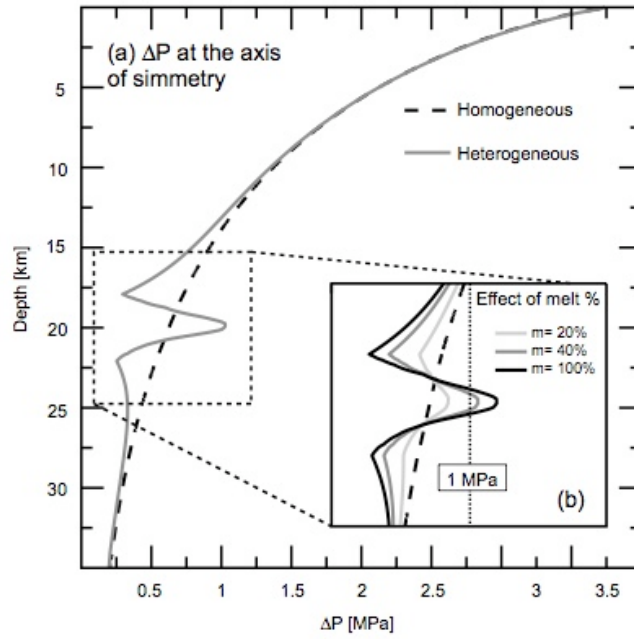


Figure DR1: Effect of melt %. (a) Decompression amplitudes caused by the El Golfo landslide calculated on the axis of symmetry (see Fig. 2a). Results for homogeneous (dashed line) and heterogeneous (solid line) models are compared. (b) Melt percentage ($m\%$) within the magma storage zone significantly affects the mechanical response of the surrounding rock.

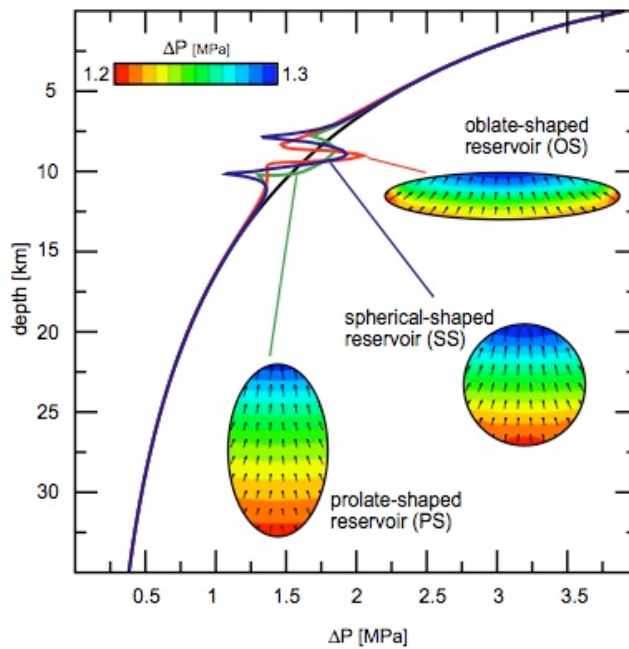


Figure DR2: Effect of shape of magma storage zone on decompression.

References

- Amelung, F., Jonsson, S., Zebker, H. and Segall, P., 2000. Widespread uplift and 'trapdoor' faulting on Galapagos volcanoes observed with radar interferometry. *Nature*, 407(6807): 993-996.
- Amoruso, A., L. Crescentini, A. T. Linde, I. S. Sacks, R. Scarpa, and P. Romano (2007), A horizontal crack in a layered structure satisfies deformation for the 2004–2006 uplift of Campi Flegrei, *Geophysical Research Letters*, 34, L22313.
- Amoruso, A., L. Crescentini, and G. Berrino (2008), Simultaneous inversion of deformation and gravity changes in a horizontally layered half-space: Evidences for magma intrusion during the 1982-1984 unrest at Campi Flegrei caldera (Italy), *Earth and Planetary Science Letters*, 272(1-2), 181-188.
- Anderson, A.T., 1976, Magma mixing: petrological process and volcanological tool: *Journal of Volcanology and Geothermal Research*, v. 1, p. 3–33.
- Andrew, R.E. and Gudmundsson, 2007, A. Distribution, structure, and formation of Holocene lava shields in Iceland: *Journal of Volcanology and Geothermal Research*, v. 168, p. 137–15.
- Battaglia, M., C. Troise, F. Obrizzo, F. Pingue, and G. D. Natale (2006), Evidence for fluid migration as the source of deformation at Campi Flegrei caldera (Italy), *Geophysical Research Letters*, 33, L01307.
- Beauducel, F., G. D. Natale, F. Obrizzo, and F. Pingue (2004), 3-D Modelling of Campi Flegrei Ground Deformations: Role of Caldera Boundary Discontinuities, *Pure and Applied Geophysics*, 161(7), 1329-1344.
- Bell, F.G., 2000. *Engineering properties of soils and rocks*. Blackwell, London.
- Bellucci, F., J. Woo, C. R. J. Kilburn, and G. Rolandi (2006), Ground deformation at Campi Flegrei, Italy: implications for hazard assessment, *Geological Society, London, Special Publications*, 269(1), 141-157.
- Berardino, P., G. Fornaro, R. Lanari, and E. Sansosti (2002), A new algorithm for surface deformation monitoring based on small baseline differential SAR interferograms, *Geoscience and Remote Sensing, IEEE Transactions*, 40(11), 2375-2383.
- Bianco, F., E. Del Pezzo, G. Saccorotti, and G. Ventura (2004), The role of hydrothermal fluids in triggering the July-August 2000 seismic swarm at Campi Flegrei, Italy: evidence from seismological and mesostructural data, *Journal of Volcanology and Geothermal Research*, 133(1-4), 229-246.

Blake, S., 1981, Volcanism and the dynamics of open magma chambers: *Nature*, v. 289, p. 783–785.

Bodnar, R. J., C. Cannatelli, B. De Vivo, A. Lima, H. E. Belkin, and A. Milia (2007), Quantitative model for magma degassing and ground deformation (bradyseism) at Campi Flegrei, Italy: Implications for future eruptions, *Geology*, 35(9), 791-794.

Bonafede, M. (1991), Hot fluid migration: an efficient source of ground deformation: application to the 1982-1985 crisis at Campi Flegrei-Italy, *Journal of Volcanology and Geothermal Research*, 48(1-2), 187-198.

Brocher, T. M. (2005), Empirical Relations between Elastic Wavespeeds and Density in the Earth's Crust, *Bulletin of the Seismological Society of America*, 95(6), 2081-2092.

Carracedo, J.C. et al., 2001, Geology and volcanology of La Palma and El Hierro, western Canaries: *Estudios Geológicos*, v. 57, p. 175-273.

Casu, F., M. Manzo, and R. Lanari (2006), A quantitative assessment of the SBAS algorithm performance for surface deformation retrieval from DInSAR data, *Remote Sensing of Environment*, 102(3-4), 195-210.

Cayol, V., e F. H. Cornet (1998), Effects of Topography on the Interpretation of the Deformation Field of Prominent Volcanoes - Application to Etna, *Geophysical Research Letters*, 25(11), 1979–1982.

Cheng, C. H., and D. H. Johnston (1981), Dynamic and Static Moduli, *Geophysical Research Letters*, 8(1), 39–42.

Chiarabba, C., and M. Moretti (2006), An insight into the unrest phenomena at the Campi Flegrei caldera from Vp and Vp/Vs tomography, *Terra Nova*, 18(6), 373-379.

Chiodini, G., F. Frondini, C. Cardellini, D. Granieri, L. Marini, and G. Ventura (2001), CO₂ degassing and energy release at Solfatara volcano, Campi Flegrei, Italy, *Journal of Geophysical Research*, 106(B8), 16,213–16,221.

Chiodini, G. (2009), CO₂/CH₄ ratio in fumaroles a powerful tool to detect magma degassing episodes at quiescent volcanoes, *Geophys. Res. Lett.*, 36, L02302.

Crescentini, L., and A. Amoroso (2007), Effects of crustal layering on the inversion of deformation and gravity data in volcanic areas: An application to the Campi Flegrei caldera, Italy, *Geophysical Research Letters*, 34, L09303.

Danyushevsky, L. V., 2001, The effect of small amounts of H₂O on crystallisation of mid-ocean ridge and backarc basin magmas: *Journal of Volcanology and Geothermal Research*, v. 110, p. 265–280.

De Natale, G., F. Pingue, P. Allard, and A. Zollo (1991), Geophysical and geochemical modelling of the 1982-1984 unrest phenomena at Campi Flegrei caldera (southern Italy), *Journal of Volcanology and Geothermal Research*, 48(1-2), 199-222.

De Natale, G., C. Troise, F. Pingue, G. Mastrolorenzo, L. Pappalardo, M. Battaglia, and E. Boschi (2006), *The Campi Flegrei caldera: unrest mechanisms and hazards*, Geological Society, London, Special Publications, 269(1), 25-45.

De Vivo, B. (2006), *Volcanism in the Campania Plain*, Elsevier, Amsterdam, 324 p.

Deino, A. L., G. Orsi, S. de Vita, and M. Piochi (2004), The age of the Neapolitan Yellow Tuff caldera-forming eruption (Campi Flegrei caldera - Italy) assessed by $^{40}\text{Ar}/^{39}\text{Ar}$ dating method, *Journal of Volcanology and Geothermal Research*, 133(1-4), 157-170.

Dieterich, J.H., Decker, R.W., 1975. Finite element modelling of surface deformation associated with volcanism, *Journal of Geophysical Research*, 80(29):4,094–4,102.

Dixon, J.E., Clague, D.A., Wallace, P., and Poreda, R., 1997, Volatiles in alkalic basalts from the North Arch volcanic field, Hawaii: extensive degassing of deep submarine-erupted alkalic series lavas: *Journal of Petrology*, v. 38, p. 911–939.

Du, Y., P. Segall, and H. Gao, 1997. Quasi-static dislocations in three dimensional inhomogeneous media. *Geophysical Research Letters*, 24: 2347–2350.

Dzurisin, D., 2006, *Volcano Deformation: Geodetic Monitoring Techniques*, Berlin, Springer, Springer-Praxis Books in Geophysical Sciences, 441 p.

Fagan, M. J., 1992, *Finite Element Analysis: Theory and Practice*: Longman.

Fialko, Y., Y. Khazan, and M. Simons (2001), Deformation due to a pressurized horizontal circular crack in an elastic half-space, with applications to volcano geodesy, *Geophysical Journal International*, 146(1), 181-190.

Ginibre, C. and Wörner, G., 2007, Variable parent magmas and recharge regimes of the Parinacota magma system (N. Chile) revealed by Fe, Mg and Sr zoning in plagioclase: *Lithos* v. 98, p. 118–140.

Gee, M. J. R., Watts, A. B., Masson, D. G. and Mitchell, N. C., 2001, Landslides and the evolution of El Hierro in the Canary Islands: *Marine Geology*, v. 177, p. 271–293.

Geist, D., Howard, K.A., Jellinek, A.M. and Rayder, S., 1994. The volcanic history of Volcano Alcedo, Galápagos Archipelago: A case study of rhyolitic oceanic volcanism. *Bulletin of Volcanology*, 56(4): 243-260.

Geist, D., Chadwick, W. and Johnson, D., 2006. Results from new GPS and gravity monitoring networks at Fernandina and Sierra Negra Volcanoes, Galapagos, 2000-2002, *Journal of Volcanology and Geothermal Research*, 150, 1-3, 79-97.

Goodman, R.E., 1989. *Introduction to rock mechanics*. Wiley, New York.

Gottsmann, J., A. G. Camacho, K. F. Tiampo, and J. Fernandez (2006), Spatiotemporal variations in vertical gravity gradients at the Campi Flegrei caldera (Italy): a case for source multiplicity during unrest?, *Geophysical Journal International*, 167(3), 1089-1096.

Gudmundsson, A., 1988, Effect of tensile stress concentration around magma chambers on intrusion and extrusion frequencies: *Journal of Volcanology and Geothermal Research*, v. 35, p. 179–194.

Gudmundsson, A., Loetveit, I.F., 2005. Dyke emplacement in a layered and faulted rift zone, *Journal of Volcanology and Geothermal Research*, 144, 1-4, 311-327.

Gudmundsson, A., 2006. How local stresses control magma-chamber ruptures, dyke injections, and eruptions in composite volcanoes. *Earth-Science Reviews*, 79(1-2): 1-31.

Hansteen, T.H., Klügel, A., and Schmincke, H.U., 1998, Multi-stage magma ascent beneath the Canary Islands: Evidence from fluid inclusions: *Contributions to Mineralogy and Petrology*, v. 132, p. 48–64.

Heap, M.J., S. Vinciguerra, and P. Meredith (2008) in press, The evolution of elastic moduli with increasing crack damage during cyclic stressing of a basalt from Mt. Etna volcano, *Tectonophysics*.

Hildenbrand, A., Gillot, P. and Le Roy, I., 2004, Volcano-tectonic and geochemical evolution of an oceanic intra-plate volcano: Tahiti-Nui (French Polynesia): *Earth and Planetary Science Letters*, v. 217, p. 349–365.

Hoernle, K., and Schmincke, H.-U., 1993, The role of partial melting in the 15-Ma geochemical evolution of Gran Canaria: A blob model for the Canary Hotspot: *Journal of Petrology*, v. 34, p. 599–626.

Holland, J. H. (1975), *Adaptation in natural and artificial systems*, University of Michigan press, Ann Arbor.

Hooper, A., Segall, P., Johnson, K. and Rubinstein, J., 2002. Reconciling seismic and geodetic models of the 1989 Kilauea south flank earthquake. *Geophysical Research Letters*, 29(22): 19-1 - 19-4.

Hora, J. M., Singer, B. S. and Wörner G., 2007, Volcano evolution and eruptive flux on the thick crust of the Andean Central Volcanic Zone: $^{40}\text{Ar}/^{39}\text{Ar}$ constraints from Volcan Parinacota, Chile: *Geological Society of America Bulletin* v. 119, p. 343–362.

Huppert, H. E., and Woods, A. W., 2002, The role of volatiles in magma chamber dynamics: *Nature*, p. 420, v. 493–495.

Izbekov, P., Eichelberger, J., Belousova, M. and Ozerov, A., 2006, Post-collapse trends at Bezymianny Volcano, Kamchatka, Russia and the May 6, 2006 eruption: *AGU Fall Meeting Abstracts*, 11, B-0576.

Jónsson, S., H. Zebker, P. Cervelli, P. Segall, H. Garbeil, P. Mouginiis-Mark, and S. Rowland, 1999. A shallow-dipping dike fed the 1995 Flank Eruption at Fernandina Volcano, Galapagos, observed by Satellite Radar Interferometry. *Geophysical Research Letters*, 26: 1077-1080.

Jónsson, S., Zebker, H., and Amelung, F., On trapdoor faulting at Sierra Negra volcano, Galapagos, *Journal of Volcanology and Geothermal Research*, 144, 1-4, 59-71.

Jull, M. and McKenzie, D., 1996, The effect of deglaciation on mantle melting beneath Iceland: *Journal of Geophysical Research*, v. 101, p. 21,815–21,828.

Kanamori, H., 1972, Relation between tectonic stress, great earthquakes and earthquake swarms: *Tectonophysics*, v. 14, p. 1–12.

Klügel, A., Hansteen, T. H. and Galipp K., 2005, Magma storage and underplating beneath Cumbre Vieja volcano, La Palma (Canary Islands): *Earth and Planetary Science Letters*, v. 236, p. 211–226.

Lanari, R., P. Berardino, S. Borgström, C. Del Gaudio, P. De Martino, G. Fornaro, S. Guarino, G. P. Ricciardi, E. Sansosti, and P. Lundgren (2004), The use of IFSAR and classical geodetic techniques for caldera unrest episodes: application to the Campi Flegrei uplift event of 2000, *Journal of Volcanology and Geothermal Research*, 133(1-4), 247-260.

Lipman, P.W., Rhodes, J.M. and Dalrymple, G.B., 1991, The Ninole Basalt — Implications for the structural evolution of Mauna Loa volcano, Hawaii: *Bulletin of Volcanology*, v. 53, p. 1–19.

Longpré, M., Troll, V. R. and Hansteen T. H., 2008, Upper mantle magma storage and transport under a Canarian shield-volcano, Teno, Tenerife (Spain): *Journal of Geophysical Research*, v. 113, B-08203.

Lundgren, P., S. Usai, E. Sansosti, R. Lanari, M. Tesauro, G. Fornaro, and P. Berardino (2001), Modeling surface deformation observed with synthetic aperture radar interferometry at Campi Flegrei caldera, *Journal of Geophysical Research*, 106(B9), 19,355–19,366.

Manga, M. and Brodsky, E., 2006, Seismic triggering of eruptions in the far field: Volcanoes and geysers: *Annual Review of Earth and Planetary Science*, v. 34, p. 263.

Manconi, A., T. R. Walter, and F. Amelung (2007), Effects of mechanical layering on volcano deformation, *Geophysical Journal International*, 170(2), 952-958.

Masson, D.G. et al., 2002, Slope failures on the flanks of the western Canary Islands: *Earth Science Reviews*, v. 57, p. 1–35.

Masterlark, T. and Z. Lu (2004), Transient volcano deformation sources imaged with interferometric synthetic aperture radar: Application to Seguam Island, Alaska, *Journal of Geophysical Research*, 109, B01401.

Masterlark, T. (2007), Magma intrusion and deformation predictions: Sensitivities to the Mogi assumptions, *Journal of Geophysical Research*, 112, B06419.

Mastrolorenzo, G., and L. Pappalardo (2006), Magma degassing and crystallization processes during eruptions of high-risk Neapolitan-volcanoes: Evidence of common equilibrium rising processes in alkaline magmas, *Earth and Planetary Science Letters*, 250(1-2), 164-181.

McCann, D. M., and D. C. Entwisle (1992), Determination of Young's modulus of the rock mass from geophysical well logs, *Geological Society, London, Special Publications*, 65(1), 317-325.

Maclennan, J. et al., 2002, The link between volcanism and deglaciation in Iceland: *Geochemistry Geophysics Geosystems*, v. 3, p. 1062.

McBirney, A.W., H., 1969. *Geology and Petrology of the Galápagos Islands*. *Mem. Geol. Soc. Am.*, 118.

McGuire, W., 1996, *Volcano instability: a review of contemporary themes*: Geological Society, London, *Special Publications*, v. 110, p. 1–23.

Moore, J. G., W. R. Normark, and Holcomb R. T., 1994, Giant Hawaiian landslides: *Annual Review of Earth and Planetary Sciences* v. 22, p. 119–144.

McTigue, D. F., 1987. Elastic stress and deformation near a finite spherical magma body: resolution of the point source paradox. *Journal of Geophysical Research*. 92, 12,931 – 12,940.

Meo, M., U. Tammaro, and P. Capuano (2008), Influence of topography on ground deformation at Mt. Vesuvius (Italy) by finite element modelling, *International Journal of Non-Linear Mechanics*, 43(3), 178-186.

Mogi, K. (1958), Relations between the eruptions of various volcanoes and the deformations of the ground surface around them, Bull. Earthquake Res. Inst. Univ. Tokyo, 36, 99–134.

Munro, D.C. and Rowland, S.K., 1996. Caldera morphology in the western Galapagos and implications for volcano eruptive behavior and mechanisms of caldera formation. *Journal of Volcanology and Geothermal Research*, 72(1-2): 85-100.

Nakagawa, M., Wada, K. and Wood, C.P., 2002, Mixed magmas, mush chambers and eruption triggers: Evidence from zoned clinopyroxene phenocrysts in andesitic scoria from the 1995 eruptions of Ruapehu Volcano, New Zealand: *Journal of Petrology*, v. 43, p. 2279–2303.

Newman, A. V., Dixon, T. H. and Gourmelen N., 2006, A four-dimensional viscoelastic deformation model for Long Valley Caldera, California, between 1995 and 2000: *Journal of Volcanology and Geothermal Research*, v. 150, p. 244–269.

Okada, Y. (1985), Surface deformation due to shear and tensile faults in a half-space, *Bulletin of the Seismological Society of America*, 75(4), 1135-1154.

Okubo, P.G., Benz, H.M. and Chouet, B.A., 1997. Imaging the crustal magma sources beneath Mauna Loa and Kilauea volcanoes, Hawaii. *Geology*, 25(10): 867-870.

Patriat, M. et al., 2002, Deep crustal structure of the Tuamotu plateau and Tahiti (French Polynesia) based on seismic refraction data: *Geophysical Research Letters*, v. 29, p. 1656.

Pepe, A., E. Sansosti, P. Berardino, and R. Lanari (2005), On the generation of ERS/ENVISAT DInSAR time-series via the SBAS technique, *Geoscience and Remote Sensing Letters*, IEEE, 2(3), 265-269.

Picozzi, M., S. Parolai, e S. M. Richwalski (2005), Joint inversion of H/V ratios and dispersion curves from seismic noise: Estimating the S-wave velocity of bedrock, *Geophysical Research Letters*, 32, L11308.

Pinel, V. and Jaupart, C., 2005, Some consequences of volcanic edifice destruction for eruption conditions: *Journal of Volcanology and Geothermal Research*, v. 145, p. 68–80.

Pinel, V. and Jaupart, C., 2000, The effect of edifice load on magma ascent beneath a volcano. *Philosophical Transactions: Mathematical, Physical and Engineering Sciences*, v. 358, p. 1515–1532.

Presley, T.K., Sinton, J.M. and Pringle, 1997, M. Postshield volcanism and catastrophic mass-wasting of the Waianae Volcano, Oahu, Hawaii: *Bulletin of Volcanology*, v. 58, p. 597–616.

Pritchard, M.E., and M. Simons, 2004. An InSAR-based survey of volcanic deformation in the central Andes. *Geochem. Geophys. Geosyst.*

Rivalta, E., Mangiavillano, W., Bonafede, M., (2002) The edge dislocation problem in a layered elastic medium, *Geophysical Journal International* 149 (2), 508–523.

Robinson, J. E., and Eakins, B. W., 2006, Calculated volumes of individual shield volcanoes at the young end of the Hawaiian Ridge: *Journal of Volcanology and Geothermal Research*, v. 151, p. 309–317.

Roth, F. (1993): Deformations in a layered crust due to a system of cracks - Modeling the effect of dike injections or dilatancy, *Journal of Geophysical Research*, 98, B3, 4543-4551.

Rowland, S.K., Harris, A.J.L., Wooster, M.J, Amelung, F., Garbeil, H., Wilson, L., and Mark, P.J.M., 2003. Volumetric characteristics of lava flows from interferometric radar and multispectral satellite data: The 1995 Fernandina and 1998 Cerro Azul eruptions in the western Galapagos. *Bulletin of Volcanology*, 65(5): 311-330.

Ryan, M.P., 1988, The mechanics and three-dimensional internal structure of active magmatic systems: Kilauea volcano, Hawaii: *Journal of Geophysical Research*, v. 93, p. 4213-4248.

Ryan, M., 1980, Mechanical behavior of magma reservoir envelopes: Elasticity of the olivine tholeiite solidus: *Bulletin of Volcanology*, v. 43, p. 743–772.

Saccorotti, G., F. Bianco, M. Castellano, and E. D. Pezzo (2001), The July-August 2000 Seismic Swarms at Campi Flegrei Volcanic Complex, Italy, *Geophysical Research Letters*, 28(13), 2525–2528.

Saccorotti, G., S. Petrosino, F. Bianco, M. Castellano, D. Galluzzo, M. La Rocca, E. Del Pezzo, L. Zaccarelli, and P. Cusano (2007), Seismicity associated with the 2004-2006 renewed ground uplift at Campi Flegrei Caldera, Italy, *Physics of The Earth and Planetary Interiors*, 165(1-2), 14-24.

Savage, J. C.: 1987, Effect of crustal layering upon dislocation modeling, *Journal of Geophysical Research*. 92, 10,595–10,600.

Schmincke, H.-U., 1998, *Gran Canaria: Geological Field Guide*, Pluto Press.

Shirzaei, M., Walter T.R, (2009) in press, Randomly Iterated Search and Statistical Competency (RISC) as powerful inversion tools for deformation source modeling: application to volcano InSAR data, *Journal of Geophysical Research*.

Siebert, L., 1984, Large volcanic debris avalanches: Characteristics of source areas, deposits, and associated eruptions: *Journal of Volcanology and Geothermal Research*, v. 22, p. 163–197.

Siebert, L., Begöt, J. E. and Glicken H., 1995, The 1883 and late-prehistoric eruptions of Augustine volcano, Alaska: *Journal of Volcanology and Geothermal Research*, v. 66, p. 367–395.

Simkin, T.S., Siebert, L., 1994. *Volcanoes of the World*. Geoscience, Tucson.

Sigvaldason, G. E., Annertz, K. and Nilsson, M., 1992, Effect of glacier loading/deloading on volcanism: postglacial volcanic production rate of the Dyngjufjöll area, central Iceland: *Bulletin of Volcanology*, v. 54, p. 385–392.

Soroush, H., and A. Fahimifar (2003), Evaluation of some physical and mechanical properties of rocks using ultrasonic pulse technique and presenting equations between dynamic and static constants, *International Society for Rock Mechanics, 10th Congress Technology roadmap for Rock Mechanics Volume 2*.

Spera, F. J., 2000, Physical properties of magma: *Encyclopedia of Volcanoes*, p. 171–190.

Stroncik, N., Klügel A. and Hansteen T., 2008, The magmatic plumbing system beneath El Hierro (Canary Islands): constraints from phenocrysts and naturally quenched basaltic glasses in submarine rocks, *Contributions to Mineralogy and Petrology*.

Tilling, R. I., and Dvorak, J. J., 1993, Anatomy of a basaltic volcano: *Nature*, v. 363, p.125–133.

Trasatti, E., C. Giunchi, and M. Bonafede (2005), Structural and rheological constraints on source depth and overpressure estimates at the Campi Flegrei caldera, Italy, *Journal of Volcanology and Geothermal Research*, 144(1-4), 105-118.

Trasatti, E. et al. (2008), The 2004–2006 uplift episode at Campi Flegrei caldera (Italy): Constraints from SBAS-DInSAR ENVISAT data and Bayesian source inference, *Geophysical Research Letters*, 35, L07308.

Trasatti, E. and Bonafede, M., (2008) in press. Gravity changes due to overpressure sources in 3D heterogeneous media, *Ann. Geophys* 51 (1).

Voight, B., Glicken, H., Janda, R. and Douglas P., 1981, Catastrophic rockslide avalanche of May 18. In P. W. Lipman and D. R. Mullineaux, *The 1980 Eruptions of Mount St. Helens*.

Walter, T. R., 2003, Buttressing and fractional spreading of Tenerife, an experimental approach on the formation of rift zones: *Geophysical Research Letters*, v. 30, p. 1296.

Walter, T.R. and Amelung, F., 2007, Volcanic eruptions following $M \geq 9$ megathrust earthquakes: Implications for the Sumatra-Andaman volcanoes: *Geology* v. 35, p. 539–542.

Watson, S., and McKenzie, D., 1991, Melt generation by plumes: A study of Hawaiian volcanism: *Journal of Petrology*, v. 32, p. 501–537.

Watters, R.J., Zimbelman, D.R. and Bowman, S.D., 2000. Rock Mass Strength Assessment and Significance to Edifice Stability, Mount Rainier and Mount Hood, Cascade Range Volcanoes. *Pure and Applied Geophysics*, 157(6-8): 957-976.

Wright, C. (2008), Station corrections for the Kaapvaal seismic network: Statistical properties and relation to lithospheric structure, *Physics of the Earth and Planetary Interiors*, 167(1-2), 39-52, doi:10.1016/j.pepi.2008.02.003.

Yang, X., P. M. Davis, and J. H. Dieterich (1988), Deformation from inflation of a dipping finite prolate spheroid in an elastic half-space as a model for volcanic stressing, *Journal of Geophysical Research*, 93(B5), 4249–4257.

Yun, S., Segall, P. and Zebker, H., 2006. Constraints on magma chamber geometry at Sierra Negra Volcano, Galapagos Islands, based on InSAR observations. *Journal of Volcanology and Geothermal Research*

Zamora, M., G. Sartoris, and W. Chelini (1994), Laboratory measurements of ultrasonic wave velocities in rocks from the Campi Flegrei volcanic system and their relation to other field data, *Journal of Geophysical Research*, 99(B7), 13,553–13,561.

Zienkiewicz, O.C., 1989. *The Finite Element Method*, 1. McGraw-Hill, London.

Zollo, A., N. Maercklin, M. Vassallo, D. D. Iacono, J. Virieux, and P. Gasparini (2008), Seismic reflections reveal a massive melt layer feeding Campi Flegrei caldera, *Geophysical Research Letters*, 35, L12306.

CURRICULUM VITAE



Dipl.-Eng. Andrea Manconi

Via Diocleziano 328, 80124 Napoli
email: manconi.a@irea.cnr.it

ANAGRAPHICAL INFORMATION

born in S.Gavino Monreale (CA) the 21.08.1978, Italian citizenship, resident in Napoli (Italy) since 02.02.2009.

STUDIES

(1997) Scientific High School degree (56/60).

(2002) Bachelor of Science in Environmental Engineering (101/110).

(2005) Master of Science in Environmental Engineering (106/110).

STAGES

(*March - July 2002*) Laboratory of geotechnics by Dipartimento di Geingegneria e Tecnologie Ambientali dell'Università di Cagliari (DIGITA-CNR, Italy), during his Bachelor of Science thesis. In this period he acquired experience in the characterization of soils and rocks using standard (AASHTO) procedures.

(*July – September 2003*) Stage by the natural reserve “Area Marina Protetta Sinis-Mal di Ventre (OR, Italy). During this period he developed a project of evaluation and monitoring of the carrying capacity of several beaches of the west Sardinian coast.

(*October 2004 - March 2005*) Visiting student by the Department of Applied Geology at the Cristhian-Albrecht University of Kiel (Germany). During this period he actively participated to the project “Virtual Aquifer”, acquiring experience in numerical modeling techniques, particularly on the reactive transport and the natural of pollutants in the subsoil. This has been the topic of his Master of Science Thesis.

WORK EXPERIENCE

(November 2005 - January 2009) Guest researcher by the Department of Natural Disasters and Early Warning of the Helmholtz Centre of Geoscience GFZ Potsdam (Germany). During this period he participated to the research activity of the group "Physics of Volcanoes" under the supervision of Dr. Thomas Walter. He acquired experience in the analysis and interpretation of geodetic data (Leveling, GPS, InSAR) using analytical and numerical modeling techniques, in particular the finite element method (FEM) and the boundary element method (BEM).

(since February 2009) Post-Doc by the Italian National Council of Research (CNR), Istituto per il Rilevamento Elettromagnetico dell'Ambiente. Numerical modeling of geodetic data measured in volcanic and seismogenic areas using SAR Interferometry. Supervision of Dr. Eng. Riccardo Lanari and Dr. Eng. Eugenio Sansosti.

LANGUAGES SKILLS

Italian: Native.

English: Fluent speaking and writing. IELTS (International English Language Testing System) overall band score 6.5 acknowledged by the British Council and by the Cambridge University.

German: Very good speaking skills, good in reading and writing.

French: Good general knowledge of the language.

Spanish: Good general knowledge of the language.

COMPUTER SKILLS

Very good hardware/software basis, independent on configuration and setting of the system.

Operative Systems: Dos/Windows, Unix/Linux, Macintosh.

Software: Office (Word, Excel, Power Point, Front Page), Email and Internet.

Programming languages: C/C++, Fortran (basic), Python (basic), HTML e PHP (basic).

Technical Softwares: Matlab, Abaqus (FEM), Comsol Multiphysics (FEM), Poly3D (BEM), AutoCAD, GID, Surfer.

Graphics Software: Adobe Photoshop, Adobe Illustrator.

Other Softwares: VMWare (Virtual Machine environment), PSGRN/PSCMP (fortran based, Analysis of co-seismic and post-seismic stress/deformation), TBC (fortran based, Reactive transport in aquifers)

OTHER EXPERIENCES

(2006) Participation at the “Volcanology Summer School” organized by Prof. H.-U. Schmincke in the Canary Islands (Gran Canaria, Spain). During this period he acquired experience on detailed geological mapping of volcanic areas.

(2007) Participation to several campaigns for the installation of local seismic networks for ambient noise monitoring.

(2007) Organization board of the international workshop “2nd Geoscientific Abaqus Workshop” organized and held at the GFZ Potsdam. Scientific program, realization and management of the related website.

(2007) Teaching assistant at University of Potsdam (Germany), for the course “Volcanology”. Organization and assistance during the final excursion by the Italian volcanoes of Vesuvius, Campi Flegrei, Stromboli, Lipari, Salina and Vulcano.

(2008) Field assistance and collaboration to the project of seismic and geodetic monitoring of the volcanic area Cordon del Azúfre and Lastàrria Volcano (North Chile).

(2006/2007/2008) Organization of the stand “Volcanic Processes” during the “Long Night of Science” organized at GFZ Potsdam.

(2006-2008) Assistance to students during their stage period and/or their bachelor/ master thesis project.

PUBLICATIONS (ISI)

Schäfer, D., **Manconi, A.**, Grandel, S. & Dahmke, A., (2005), “Consequences of Different Kinetics Approaches for Simulation of Microbial Degradation on Contaminant Plume Development”, in *Reactive Transport in Soil and Groundwater*, Gunnar Ntzmann, Paolo Viotti and Per Aagaard, 127-139, Springer.

Manconi, A., Walter, T.R. & Amelung, F., (2007), “Effects of Mechanical Layering on Volcano Deformation”, *Geophysical Journal International*, Vol. 170 (2), 952-958. Times cited: 5

J. Ruch, **A. Manconi**, G. Zeni, G. Solaro, A. Pepe, T.R. Walter & R. Lanari, (2008), "Stress Transfer in the Lazufre volcanic area, Central Andes", *submitted to Geophysical Research Letters*.

A. Manconi, M.-A. Longpré, T.R. Walter, V.R. Troll, & T. Hansteen, "The effects of flank collapses on volcano plumbing systems", *submitted to Geology*.

A. Manconi, T.R. Walter, M. Manzo, G. Zeni, P. Tizzani, E. Sansosti & R. Lanari, "The source of the ground deformation at Campi Flegrei caldera during the last sixteen years: insights from Finite Element modeling and SBAS-DInSAR time series analysis", *submitted to Journal of Geophysical Research*.

CONTRIBUTIONS TO INTERNATIONAL CONFERENCES

D. Schäfer, **A. Manconi** & A. Dahmke (2004), "Identification and Consequences of Different Kinetic Approaches for Simulation of Microbial Degradation", COST 629 Workshop: Saturated & Unsaturated Zone, Integration of Process Knowledge into Effective Models, Rome 5-7 May 2004 (*oral presentation*).

A. Manconi & T.R. Walter (2006), "Mechanical heterogeneities in volcanoes analyzed with finite element models", TSK11 Volcano-Tectonics meeting, Göttingen, 21 March 2006 (*oral presentation*).

A. Manconi & T.R. Walter (2006), "The importance of mechanical heterogeneities on stress redistribution from and to volcanoes", EGU meeting, Geophysical Research Abstracts Vienna, 7 April 2006, (*poster*).

A. Manconi, T.R. Walter & F. Amelung (2006), "Heterogeneous finite element simulations of surface deformation on Darwin volcano: understanding volcano unrest", Geologische Vereinigung International Workshop, Potsdam, 26 September 2006 (*poster*).

A. Manconi, T.R. Walter & F. Amelung (2006), "Heterogeneous finite element simulations of surface deformation on Darwin volcano: understanding volcano unrest", 1st Geoscientific Abaqus Workshop, Bochum, 4 October 2006 (*poster*).

A. Manconi, T.R. Walter, & F. Amelung (2007), "Deformation due to an inflation source in a layered half-space: Application to Darwin volcano, Galápagos", EGU meeting, Geophysical Research Abstracts, Vienna, 16 April 2007 (*oral presentation*).

L. Lungarini, **A. Manconi**, T.R. Walter, C. Troise & G. De Natale, "The influence of topography and volcano tectonic structures on the ground deformation field at Vesuvius volcano", EGU meeting, Geophysical Research Abstracts, Vienna, 16 April 2007 (*oral presentation*).

A. Manconi, T.R. Walter & F. Amelung (2007), "Interaction of volcanic activity at Vesuvius and Campi Flegrei caldera", Geologische Vereinigung International workshop, Bremen, 4 October 2007 (*oral presentation*).

A. Manconi, T.R. Walter, M.-A. Longpré & V. Troll (2007), "Effects of Giant Landslides on Magma Storages: Insights from Finite Element Modeling", 2nd Geoscientific Abaqus Workshop, Potsdam, 11 October 2007 (*poster*).

M. Shirzaei, T.R. Walter, M. Motagh, **A. Manconi** & Riccardo Lanari (2007), "Inversion of InSAR data via Genetic Algorithm and Simulated Annealing methods: first results from the Campi-Flegrei volcanic region", Fringe 2007 Workshop of the European Space Agency, Frascati, December 2007 (*poster*).

A. Manconi, T.R. Walter, M.-A. Longpré & V. Troll (2008), "Effects of Giant Landslides on Magma Storages: Insights from Finite Element Modeling", VMMSG meeting, Dublin, 4 January 2008 (*poster*).

M.-A. Longpré, V. Troll, T. Hansteen, **A. Manconi** & T.R. Walter (2008), "Upper mantle magma plumbing at the Miocene Teno volcano, Tenerife", VMMSG meeting, Dublin, 4 January 2008 (*oral presentation*).

A. Manconi, T.R. Walter, M.-A. Longpré & V. Troll (2008), "Changes on plumbing system caused by volcanic sector collapses studied through finite element models", IAVCEI meeting, Reykjavik, 21 August 2008 (*oral presentation*).

A. Manconi & T.R. Walter (2008), "Effects of 3-D heterogeneities on the deformation signal detected at Campi Flegrei caldera (Southern Italy)", IAVCEI meeting, Reykjavik, 21 August 2008 (*poster*).

J. Ruch, T.R. Walter & **A. Manconi** (2008), "Volcanic slope displacements in the Lazufre area in South America revealed by satellite observation (InSAR)", Geologische Vereinigung International Workshop, Aachen, 4 October 2008 (*poster*).

V. Magni, **A. Manconi**, P. Tizzani, M. Battaglia & T.R. Walter (2008), "Heterogeneous Axial Symmetric Crustal Deformation Model for Long Valley Caldera, California", COMSOL European Conference, Hannover, 06 November 2008 (*oral presentation*).

T.R. Walter, M. Shirzaei, **A. Manconi**, J. Ruch, M. Motagh, R. Wang & J. Zschau (2008), "InSAR derived deformation source characteristics at volcanoes – how realistic are the models?", USEReST 2008 meeting, Napoli, 11 November 2008 (*oral presentation*).

A. Manconi, T.R. Walter, M. Manzo, G. Zeni, P. Tizzani, E. Sansosti & R. Lanari (2009), "The source of the ground deformation at Campi Flegrei caldera during the last sixteen years: insights from Finite Element modeling and SBAS-DInSAR time series analysis", EGU meeting, Geophysical Research Abstracts, Vienna, 19 April 2009 (*oral presentation*).

INVITED TALKS, SEMINARS and LECTURES

(26.02.2009) Advanced finite element modeling in volcano-geodesy problems. Workshop: The use of Comsol Multiphysics on Earth Science. University "La Sapienza", Roma, (*invited lecture*).

AWARDS

(2004) Scholarship SOCRATES - ERASMUS.

(2006) Scholarship "Master and Back" financed by the Sardinian regional government.

(2006) Geologische Vereinigung 2006, 1° prize, best outstanding poster.

(2006) GFZ PhD Day 2006, 3° prize, best outstanding poster.

(2007) GFZ PhD Day 2007, poster audience prize.

